Stratigraphy and Chronology of Sodicho Rockshelter – A New Sedimentological Record of Past Environmental Changes and Human Settlement Phases in Southwestern Ethiopia

Elena A. Hensel[1]*, Ralf Vogelsang[2], Tom Noack[2] and Olaf Bubenzer[3]

[1]Institute of Geography, University of Cologne, Cologne, Germany, [2]Institute of Prehistoric Archaeology, University of Cologne, Cologne, Germany, [3]Institute of Geography and Heidelberg Center for the Environment (HCE), Heidelberg University, Heidelberg, Germany

The preservation of archaeological remains and environmental information in a sediment accumulation can vary in caves and rockshelters, depending on external climatic conditions, and the circumstances within the shelter. Several sediment stratigraphies in the Horn of Africa are characterized by erosion layers, discordances and chronological gaps, that create uncertainties about the impact of climatic and environmental shifts on human settlements. Archaeological sites in Ethiopia that preserve information about human occupation during the Upper Pleistocene and Holocene often deal with major gaps during a period corresponding to MIS 2. In this study we present the first results of sedimentological, geochemical analyses and radiocarbon dating at Sodicho Rockshelter (1930 m above sea level) that provide evidence on high altitude settlement during this mentioned chronostratigraphic gap and subsequent time slices. This new archaeological site in the southwestern Ethiopian Highlands hosts a 2-m-long sediment record. So far, a stratigraphy has been excavated that dates back to ~27 ka, including several settlement phases of Late Pleistocene and Holocene hunter-gatherers and providing information on environmental changes. A multiproxy approach was chosen to establish a first general stratigraphy of the site and to disentangle the sediment composition as well as site formation processes. The results suggest a variation of allochthonous and autochthonous geogenic deposits, and anthropogenic accumulation processes. With the help of radiocarbon dating, anthropogenic layers were dated covering the arid Last Glacial Maximum (LGM, ~21 ± 2 ka). The occupation phases were interrupted in cause of environmental changes. The most prominent is the accumulation of reddish, archaeological sterile deposits that can be chronologically associated with the African Humid Period (AHP, ~15–5 ka BP). Geochemical records point to dry spells within this humid phase, suggesting correlations with regional climate signals of lacustrine sediments. These sediment accumulations of past wet conditions are covered by alternating layers of Holocene volcanic fallout and sediments with preserved cultural material. Our study

provides a preliminary impression of still poorly understood time periods of human occupation in the southwestern Ethiopian Highlands. The data obtained from Sodicho Rockshelter could validate the current state of knowledge and partially reduce the chronostratigraphic gap.
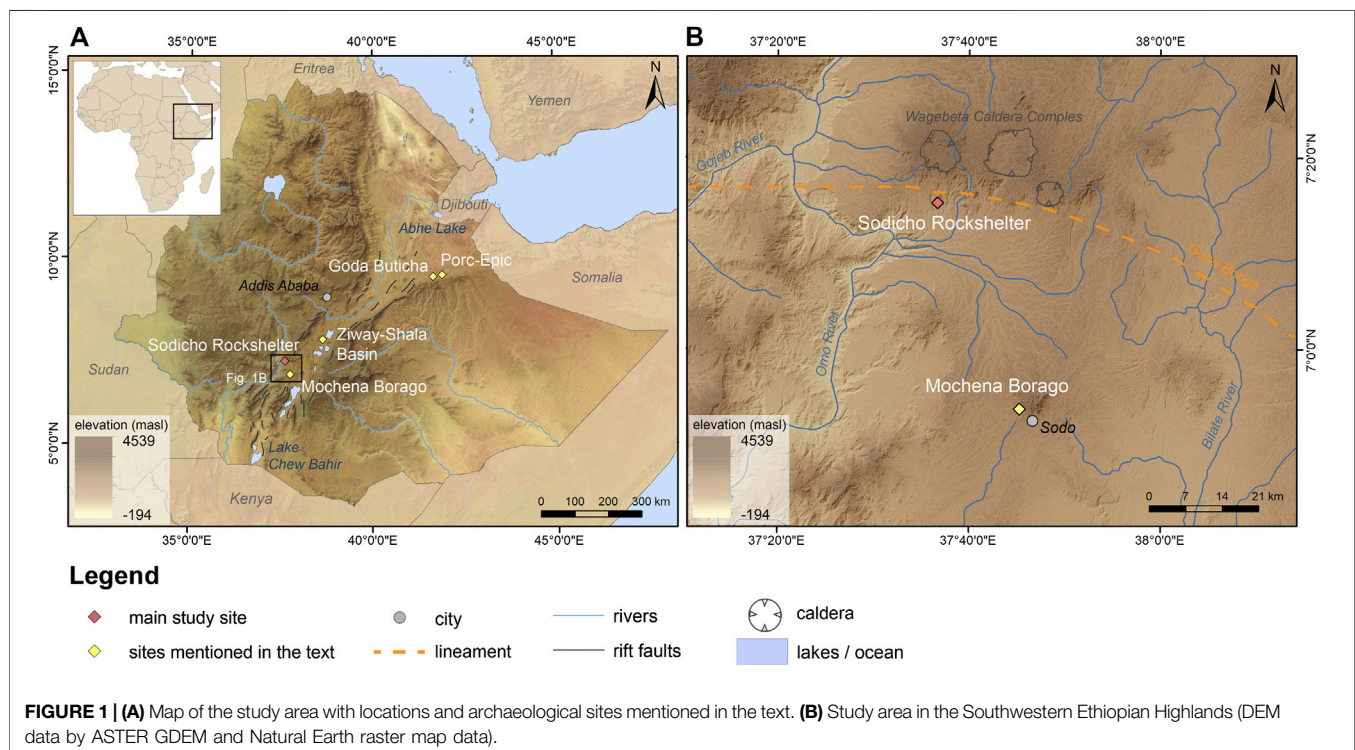
INTRODUCTION

The development of a sediment stratigraphy within a rockshelter setting is driven by diverse sediment origins and changing conditions of the regional environment, including human agency. The different sediment sources, e.g., geogenic (autochthonous and allochthonous), anthropogenic, and biogenic often result in a diverse, intermitted deposition. Like caves, rockshelters function as a sediment trap, however, they are often partly or completely exposed to weather conditions, which in turn explains the variability in deposition. The prehistoric humans used these places as natural shelters (Mentzer, 2017). The use of caves and rockshelters by prehistoric humans has been part of geoarchaeological research in several regions, such as southern and northern Africa, Europe or the Levant (Goldberg and Bar-Yosef, 1998; Goldberg et al., 2009; Marean et al., 2010; Miller et al., 2013; Kehl et al., 2014; Klasen et al., 2018; Inglis et al., 2018). The studies investigated the natural forces contributing to deposition of sediment and the active modification of sediment structures by human activities (e.g., fireplaces, trampling and bedding) (Goldberg et al., 2009; Miller et al.,

2013). Deposits can be altered, masked or even erased from the sedimentary record by post-depositional processes, resulting in gaps of knowledge and uncertainties leading to rather short and discontinuous archaeological sequences (Kuehn and Dickson, 1999). In the Horn of Africa, especially in Ethiopia, these gaps in stratification are quite common. In most cases, they correlate with the transition from the Middle Stone Age (MSA) to the Late Stone Age (LSA) during the period of the MIS 2 (Tribolo et al., 2017). Several studies at sites such as Goda Buticha, the Ziway-Shala basin and Mochena Borago identified a stratigraphical and a chronological gap, spanning from ~38 ka and reaching into the Holocene (**Figure 1A**) (Tribolo et al., 2017).

Although terrestrial paleoenvironmental records are very scarce in Ethiopia, they provide a useful source for the reconstruction of past varying environmental conditions. Lacustrine sediments from Ethiopian and Kenyan lakes refer to hyper arid conditions during the Heinrich Events (H) and the Late Glacial Maximum (LGM, ~21 ± 2 ka), followed by overall moist conditions of the African Humid Period with intermediate dry spells (Mark and Osmaton, 2008; Junginger and Trauth, 2013; Foerster et al., 2015). Higher

FIGURE 1 | (A) Map of the study area with locations and archaeological sites mentioned in the text. **(B)** Study area in the Southwestern Ethiopian Highlands (DEM data by ASTER GDEM and Natural Earth raster map data).

moisture availability in the highlands could have permitted the survival of vegetation, animals and humans during the arid phases. In this case, rockshelters in high altitude regions might have attracted hunter-gatherers, despite the challenging conditions for human physiology (Foerster et al., 2015; Vogelsang and Wendt, 2018).

Sodicho Rockshelter is located about 40 km NW from the aforementioned Mochena Borago Rockshelter site, which is one of the archaeological key-sites in northeastern Africa and shares a comparable well-structured sedimentological and archeological sequence (Brandt et al., 2017; Hensel et al., 2019). With this study we introduce preliminary results of geoarchaeological and archaeological investigations of Sodicho Rockshelter and relate the results to regional climatic records. We attempt to reconstruct geogenic and biogenic site formation processes and to compare them to the cultural induced processes. The aim of this study is 1) to determine the sediment composition, 2) to reconstruct the site formation processes in the shelter, 3) to develop a first ^{14}C chronology and 4) put the human occupation in the context of the geoarchaeological results.

BACKGROUNDS

Geoarchaeological Research

Until now, the most important rockshelter in the southwestern Ethiopian Highlands is Mochena Borago on Mount Damota. Since 1998, several research teams investigated almost 2 m of stratified Holocene and Late Pleistocene deposits. The latter preserved cultural remains dating between 36 and >50 ka (Gutherz et al., 2002; Fisher, 2010; Brandt et al., 2012; Brandt et al., 2017). In 2009 the Collaborative Research Center 806 (CRC 806, http://www.sfb806.uni-koeln.de) joint the investigations of Steven Brandt (Southwest Ethiopia Archaeological Project) at Mochena Borago. Geoarchaeological research at Mochena Borago aimed to reconstruct site formation processes with the help of geomorphological investigations and micromorphological observations (Brandt et al., 2017). During archaeological and geomorphological surveys in the surroundings, Sodicho Rockshelter was first visited in 2012 (Brandt et al., 2017; Vogelsang and Wendt, 2018; Hensel et al., 2019). Further research in the area focused on the exposure of archaeological records along the valleys of the Bilate River and its tributary the Bisare River, southwest of Mt. Damota. According to the studies, abundant archaeological material occurs in sediments, that are exposed by badland formation. These badlands are not older than 200 ka and hold mostly MSA and LSA obsidian artifacts. However, some sites also hold artifacts that show characteristics of the late Early Stone Age (ESA) (Benito-Calvo et al., 2007; De la Torre et al., 2007). Geomorphological–hydrological analyses around Mt. Damota and Mt. Sodicho revealed that the region is influenced by a very dynamic system of permanent and episodic river networks. The resulting soil erosion and the exposure and destruction of archaeological open-air sites and raw material outcrops emphasizes the importance of protected rockshelter stratigraphies and their potential to preserve archaeological deposits and environmental information (Hensel et al., 2019).

Geology, Geography, Climate and Vegetation of Study Area

Sodicho Rockshelter is located E 37°36'44 and N 7°15'21 in the southwestern Ethiopian Highlands. The cavity opens to the south and is situated at the slopes of Mount Sodicho at an elevation of about 1930 m above sea level (Hensel et al., 2019). The complex tectonic and volcanic structures of the Main Ethiopian Rift are situated to the west. To the east lies the deep canyon of the Omo River (**Figure 1B**). The mountain itself consists of a greyish to yellowish trachyte, and is part of a series of silicic domes, lavas and tephra that lie ~8 km south of the three circular Wagebeta Calderas. The past volcanic formations date back 3.6 to 4.2 Ma into the Pliocene and during the late phase of the rift system development in Ethiopia (WoldeGabriel et al., 1990; WoldeGabriel et al., 1992; Chernet, 2011; Hensel et al., 2019). The volcanic formations are aligned along the transverse east–west Goba-Bonga lineament, a depression that crosses the center of the Main Ethiopian Rift (Bonini et al., 2005; Corti, 2009; Corti et al., 2013). The present appearance of the area is shaped by Late Pleistocene to Holocene tectonic stress, climatic, and geomorphological changes (Benito-Calvo et al., 2007). A network of episodic and permanent streams drains down the slopes of Mt. Sodicho toward the Omo River, creating the mountain's characteristic irregular shape. The increased human influence during the last decades is visible by cleared slopes for cultivation and cattle farming (Hensel et al., 2019). The major soil type is the kaolinite rich, red colored Humic Nitisol, a fertile soil type, common in the humid tropics (Berhanu et al., 2013; IUSS Working Group WRB, 2014). The modern climate in the southwestern Ethiopian Highlands is a complex and variable system that is characterized by two rainy seasons with an average precipitation of about 2,000 mm per year. Over 50% of the annual rain in the SW Ethiopian Highlands falls in course of the "Kirmet", the main rainy season during the boreal summer (June to September). During the months November to February the region experiences the dry period with an average <50 mm per month, followed by a second weaker rainy season, the "Belg" (Fisher, 2010; Brandt et al., 2012; Hildebrand et al., 2019). These annual and inter-annual precipitation changes are connected to the interaction of the moist summer monsoon and the dry northeastern "Harmattan" wind system, resulting in changes of the north-south directed pressure gradient (Viste and Sorteberg, 2013; Nicholson, 2018). Further influences on the annual precipitation are associated with changes in sea surface temperature (SST) of the Indian Ocean, the northern shifting tropical rain belt, low-level convergences, and the Congo Air Boundary in lesser relevance (Griffiths, 1972; Segele et al., 2009; Tierney et al., 2011; Junginger and Trauth, 2013; Viste and Sorteberg, 2013; Nicholson, 2018).

Up to now, only the last 45 ka are analyzed from a drilling core in the Chew Bahir basin, which is situated ~300 km from Mount Sodicho. Its catchment area runs through the SW Highlands, which means that Chew Bahir was also affected by climatic

conditions prevailing in the highlands. According to sedimentological and geochemical investigations of these lake sediments, the past climate in the southwestern highlands has undergone arid and humid phases. A rather moist phase from 45 to 35 ka BP was followed by arid conditions (Foerster et al., 2012). During the cold and arid Marin Isotope Stage 2 (MIS 2, ~29–12 ka BP), lake levels and river catchments changed, which influenced the surrounding habitat of flora and fauna (Foerster et al., 2012; Foerster et al., 2015; Stewart and Jones, 2016). The aridity ended after 15 ka with an increase in humidity. This indicated the beginning of the Early Holocene African Humid Period, which stretched out until 5 ka and was interrupted by shorter dryer periods (Foerster et al., 2012; Foerster et al., 2015; Hildebrand et al., 2019; Trauth et al., 2019).

MATERIALS AND METHODS

Fieldwork and Archaeological Excavation

The excavations at Sodicho Rockshelter were conducted annually from 2015 to 2018. Of two 50 × 50 cm test pits in 2015, one was extended to an excavation trench with an area of four square meters, each split into 50 × 50 cm quadrants that were excavated individually (**Figure 2C**, F34/35 and G34/35). Big boulders stopped the extension of the second test pit (**Figure 2C**, E41), which was located in one of the cavities at the rear wall of the shelter. Both trenches are situated in backward areas that seem to be well protected from humidity, in terms of dripping water and trickle. Archaeological excavations followed natural stratigraphic boundaries, subdivided vertically into arbitrary spits with a maximum thickness of 5 cm. Spits never transversed natural stratigraphic boundaries, i.e. a spit definitely ended when visible sediment changes where observed during excavation. Specific archaeological features, such as hearths or pits, were excavated in the same way but separately from the surrounding matrix. No total station was available during the first fieldwork in 2015. Therefore, the grid system of the test pits was sat up with measuring tapes and leveling taken with a surveyor's level. Archaeological finds of the test pits were recovered via dry sieving in three stages, using mesh widths of 10, 5, and 2.5 mm. The closest spatial allocation of these finds is to one of the artificial spits. During the subsequent excavations all archaeological finds >5 mm were single plotted using a Leica TS02 total station and provenience information such as grid unit, depth, level and stratum, as well as material type (e.g., stone, bone, charcoal) were recorded. Each find was then bagged individually and assigned a unique identification number. The excavated sediments were dry sieved to recover smaller finds using 10-, 5-, and 2.5-mm mesh size. The total station was also employed to map each stratum, feature or natural disturbance as it was exposed, and forms recorded information on sedimentology, spatial and vertical configurations and other relevant data. In addition, plan views of each excavation spit and stratigraphic profiles were mapped on grid paper and recorded with digital photographs. The geoarchaeological fieldwork included on-site observation with an analysis of the sediment deposits (**Supplementary Table S1**) and a classification of the common

lithological composition of the bedrock in the rockshelter itself. Furthermore, several half-day surveys along the mountain flanks of Mt. Sodicho were undertaken to identify lithological changes of bedrock and geomorphological conditions of the area.
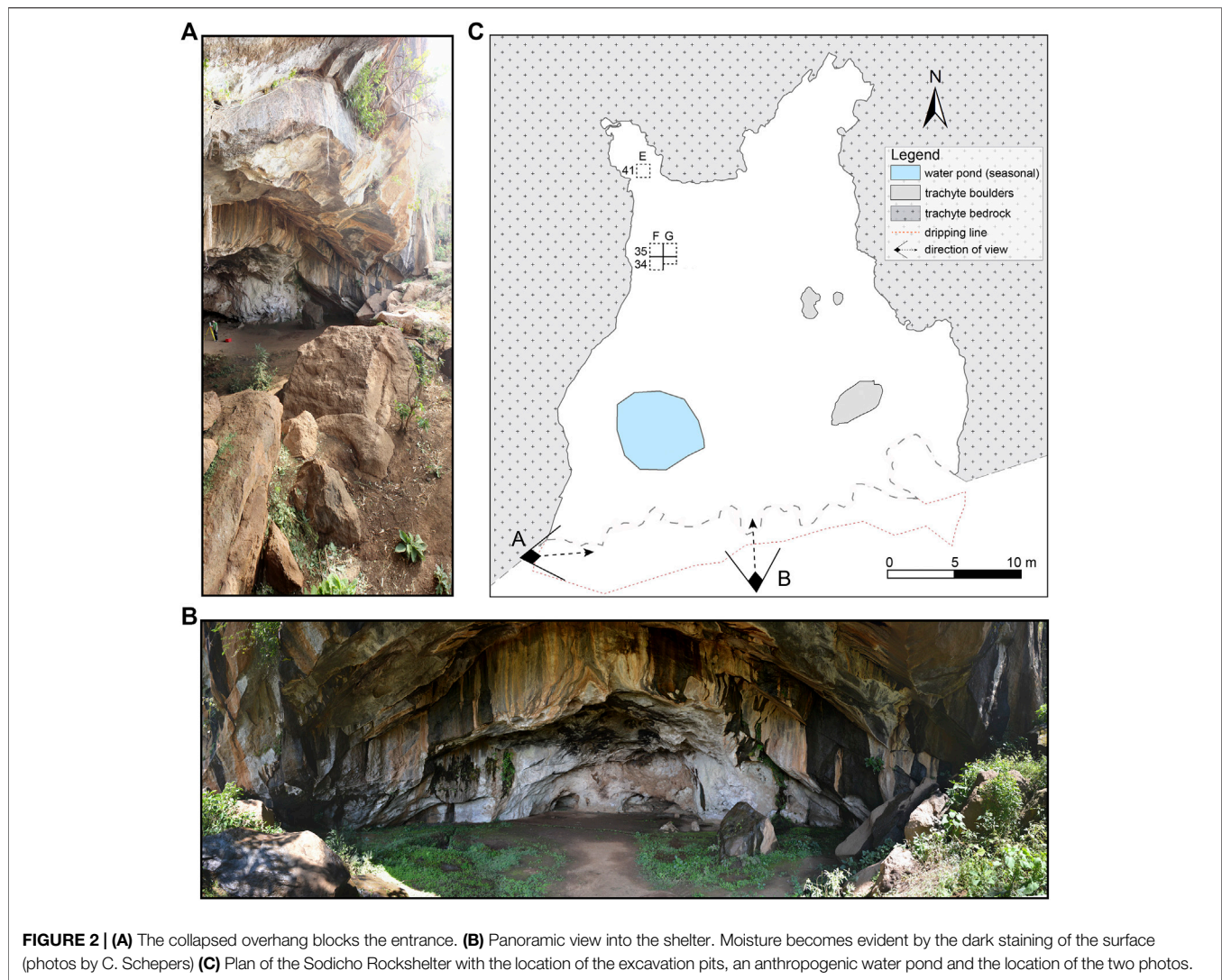
Multiproxy Sediment Analyses

Bulk sediment samples were determined with a 2 cm resolution at the west facing profile from square F35 and the south facing profile from square G35 (**Figure 3**). Lower sediment samples were taken from square G35 because collapsed blocks in F35 hindered further sampling in this square. Both sample columns overlap by approximately 30 cm. The sample thickness was increased to 4 cm in layers of difficult access, e.g., around bigger rocks. As a pre-treatment the samples were dried at 40°C in a drying chamber and sieved to remove material >2 mm.

The granulometry was determined with a Laser Diffraction Particle Size Analyzer (Beckmann Coulter LS13 320, Beckmann Coulter, Inc.) and pretreated with hydrogen peroxide (H_2O_2 15%) to remove organic opal. In addition, several reference samples were treated with hydrochloric acid (HCl 10%) to remove organic and inorganic carbon. Prior to the measurements, Na_2PO_5 (46 g/L) was applied to all samples to avoid coagulation. The results were evaluated and statistically measured with the GRADISTAT software version 8 (Blott and Pye, 2001) and the parameters are based on Folk and Ward (1957).

Sediment color was measured with a VIS spectrophotometer (Konica Minolta CM-5) to determine the reflected wavelength from the sample in a visible range of 360–740 nm and converted into $L^*a^*b^*$ values (Eckmeier and Gerlach, 2012). The $L^*a^*b^*$ values express the extinction of light in the spectra from absolute black (L^*0) to absolute white (L^*100) and the color ranges from green to red (a^* to $+a^*$) as well as from blue to yellow (b^* to $-b^*$). The redness index (RI) was calculated applying the $L^*a^*b^*$ variables according to Barrón and Torrent (1986) $RI = \frac{a^*\,(a^{*2}+b^{*2})^{\frac{1}{2}}10^{10}}{b^*\,L^{*6}}$.

The mass specific magnetic susceptibility was determined by using a Bartington MS2 Magnetic Susceptibility System with a MS2k sensor and measured twice under laboratory conditions on the sieved and weighed in samples. For further geochemical investigations a part of the material was grinded with a vibrating zircon ball mill (Mixer Mill MM 400, Retsch). The total carbon content (TC) was measured with a vario EL cube (Elementar Analysensysteme GmbH). In addition, the total organic carbon (TOC) content was measured on a few reference samples after a pretreatment of HCl (10%).

For the determination of the major and trace elemental composition two methods using X-ray fluorescence (XRF) were applied. First, all grinded samples were measured with a handheld Niton™ XL3t XRF Analyzer (Thermo Scientific™) under laboratory conditions, viz. samples were pressed in pellets and measured twice in a test stand. This method has the advantage that many samples can be measured relatively quickly and easily after a relatively complex preparation. However, studies with a portable XRF devices (pXRF) have shown that the spectrometer cannot properly measure elements like phosphorous (Hunt and Speakman, 2015).

FIGURE 2 | (A) The collapsed overhang blocks the entrance. **(B)** Panoramic view into the shelter. Moisture becomes evident by the dark staining of the surface (photos by C. Schepers) **(C)** Plan of the Sodicho Rockshelter with the location of the excavation pits, an anthropogenic water pond and the location of the two photos.

Therefore, to verify the results of the pXRF analyzer, and to derive geochemical indicators for alteration and weathering a selection of the samples were measured at the Institute of Physical Geography and Geoecology at the RWTH Aachen. Here the grinded samples were also pressed to tablets and measured twice with the SPECTRO XEPOS energy dispersive X-ray fluorescence spectrometer (Spectro). The resulting elements and oxides were then chosen as representing indicators for depositional changes. A chemical index of alteration (CIA) was calculated according to the calculations of Nesbitt and Young (1982): $CIA = \left[\frac{Al_2O_3}{Al_2O_3 + Na_2O + K_2O + CaO} \right] \times 100$.
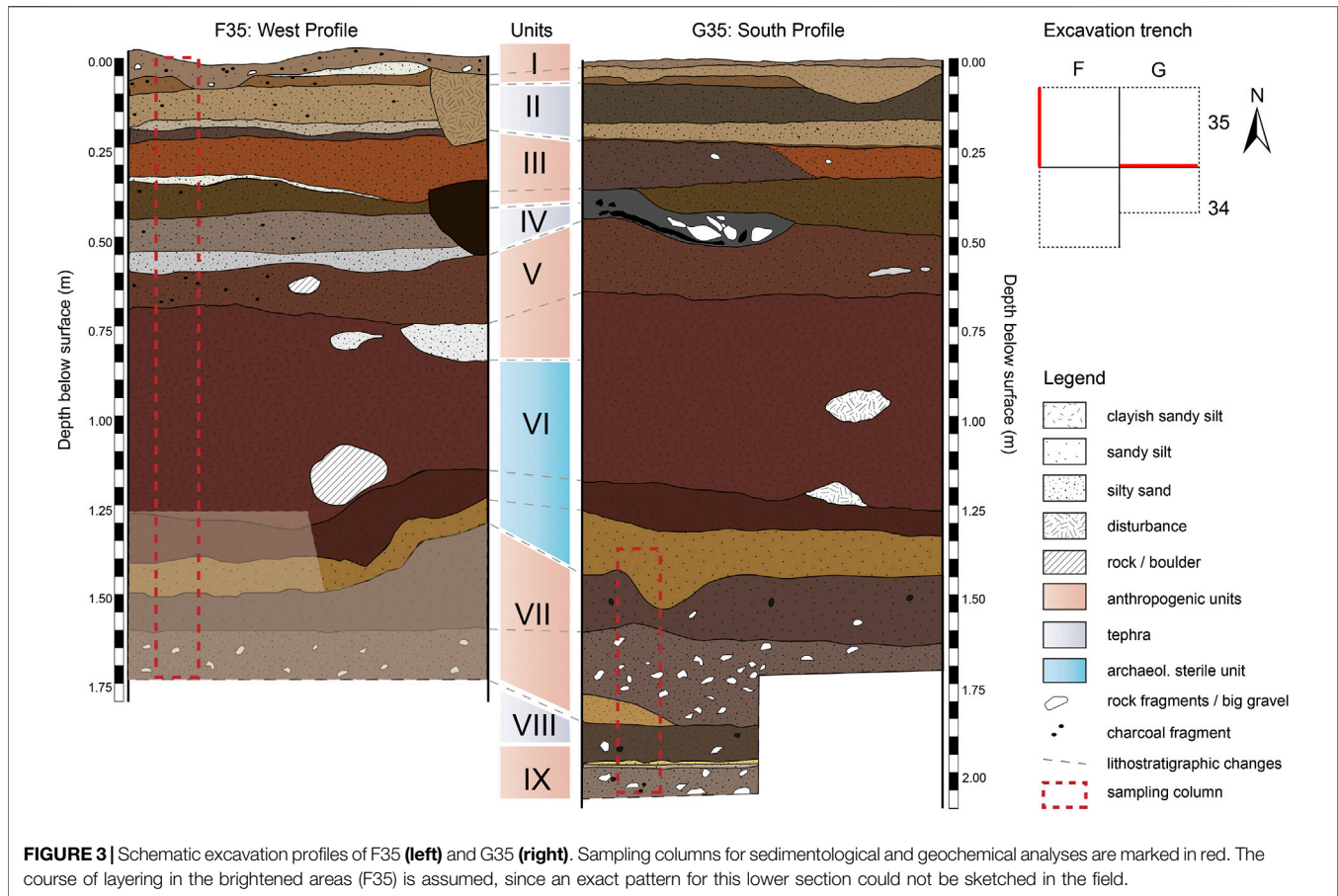
Age Determination

A total of 31 samples were collected in the squares F34, F35, and G35 during the excavations in 2015 to 2018 (**Figure 2**). The radiocarbon AMS lab Beta Analytics Limited analyzed 28 samples of seeds and charcoal. Additionally, two charcoal and one soot sample, the latter scratched from the besmoked outer face of a cooking pot sherd, were measured at the AMS laboratory of the University of Cologne. The results were calibrated with Calib8.10.

using the IntCal20.[14]C curve (Reimer et al., 2020). A classic age depth model was established with the clam2.3.5 package in RStudio according to Blaauw (2010). In the model the radiocarbon ages were calibrated with the northern hemisphere terrestrial calibration curve IntCal20.[14]C.

RESULTS

Field Observations at the Sodicho Rockshelter

The south facing opening of the rock shelter is almost completely protected by big trachytic boulders (2 diam.) that originate from the partial collapse of the originally larger front overhang (**Figure 2A**). This hinders the direct influence of precipitation and fluvial weathering into the flat shelter. However, the blocking rocks cause a slight downward slope into the shelter. The sediment accumulation therefore differs spatially, which in turn can influence the characteristics of certain sediment layers, like deposit thickness. The interior

FIGURE 3 | Schematic excavation profiles of F35 **(left)** and G35 **(right)**. Sampling columns for sedimentological and geochemical analyses are marked in red. The course of layering in the brightened areas (F35) is assumed, since an exact pattern for this lower section could not be sketched in the field.

of Sodicho Rockshelter is characterized by the effects of moisture, which seeps through cracks in the ceiling and the walls, generating dark staining on the rock surface, and creating shallow pools and drip holes with stagnant water during wet seasons (**Figure 2**). A larger water pond in the western entrance area was dug by the local population living there. Big boulders and blocks in the south eastern corner are rounded by water dripping down the roof. Low growing plants and shrubs cover certain parts of the floor and grow along fissures at the rock shelter walls. During dry season the rock shelter can dry up almost completely. Apart from the dark staining at the walls and ceiling the trachyte differs in color, crystallization and softness within the shelter. The western wall is characterized by a pale gray trachyte with a rather crumbly matrix due to granular disintegration. Distinct alveolar weathering (honeycomb weathering) is common and parts of the walls show flaking of the rock surface and uneven exfoliation of the rock surface, which creates curve surfaced boulders. The color of the trachyte changes toward the eastern wall to a mustard yellow with well crystalized and colorless potassium feldspar minerals. Several overhangs along the rock shelter walls are darkened by soot caused by human induced burning. A low and narrow cavity in the north eastern back is extremely stained by fire activity. The lower ceiling has obtained a shiny, greasy surface due to the close fire exposure.

First observations during excavation revealed a complex stratigraphy with distinguishable sediment units and prominent boundaries. Some of the sediment units (Unit I, III, V, VII and IX) correspond to archaeological layers, that contain cultural material, such as obsidian artifacts and charcoal, and human made structures, such as pits and hearth. A 60 cm thick sterile sediment deposit roughly divides the deposits and associated human occupation phases into two parts. In the upper part of the stratigraphy, the anthropogenic units alternate with lighter colored geogenic units identified as tephra. The boundaries between these units are not uniform. Whereas the boundary between a cultural layer and an overlying tephra is sharp (e.g., between Units V and VI or between III and II), the transition between a cultural layer to a subjacent tephra seems gradual (e.g., between Units IV and III or between Units II and I). The tephra layers are exclusively of geogenic origin and therefore cultural remains are absent. Intermixing only occurs when the volcanic deposits have been relocated or disturbed by subsequent construction of pits or hearths. The lower part of the stratigraphy, below the thick sterile unit, is characterized a lager rockfall deposit, followed by anthropogenic deposits and geogenic deposits. The different layers in the lower section of the stratigraphy are difficult to distinguish, due to gradual or unclear layer boundaries and even mixing of the layers. Bioturbation can be recognized sporadically as insect or rodent

FIGURE 4 | Sedimentological properties of the profile F35: lithostratigraphy according to grain size analysis and sediment color measurement; grain size distribution; particle size parameter for aeolian transport; particle size parameter: 90th and 10th percentiles; CIELab color value L*; calculated Redness Index; magnetic susceptibility; sedimentological units.

borrows in all units. There is no macroscopic evidence of rooting by plants in the excavated stratigraphy. A detailed description of each unit, with its most important components can be found in the **Supplementary Table S1**.

Multiproxy Sediment Analyses

Macroscopic investigations of the 2 m stratigraphy revealed a complex interplay of cultural layers with light colored tephras and a 60 cm thick sterile sediment deposit. With the help of sedimentological and geochemical analysis nine sedimentological units (I–X) can be systematically differentiated.
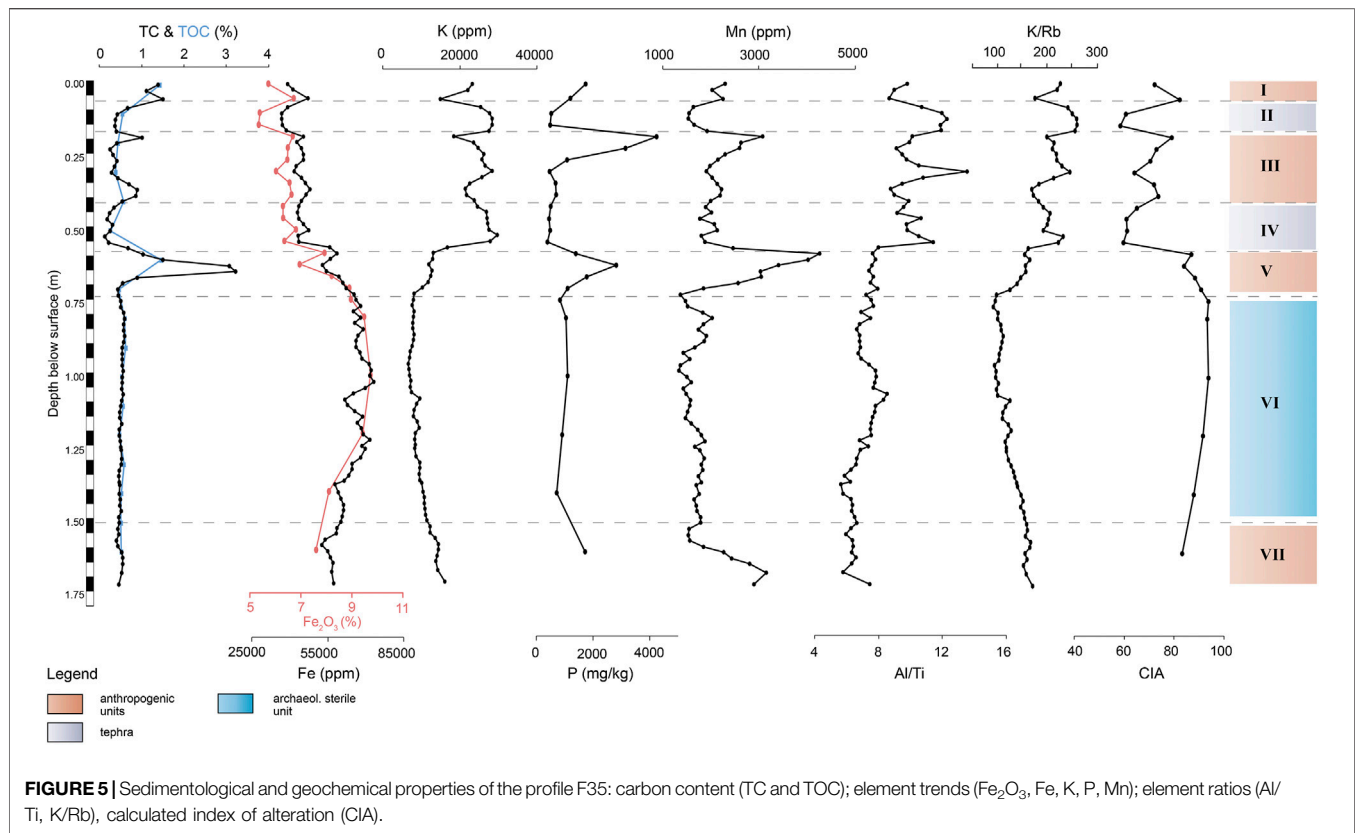
Profile F35

We measured all sediment samples with a grain-size analyses to investigate changes in particle size distribution through the whole stratigraphy. It turns out that (sandy) medium to coarse silt is the omnipresent mean fraction, although the (silty) fine sand content is increased in several layers of the upper (0.00–0.73 m) profile section. The grain size peaks in Unit IV and V. The graph in **Figure 4** shows that the clay content increases suddenly within the sterile layer of Unit VI. According to the statistical analyses, the sample curves show a bi- and polymodal distribution and overall very poor sorting. The amount of the grain size fractions that corresponds to aeolian transport, e.g., fine sand and very coarse silt (40–125 μm), ranges from 9 to 41% with peaks in Unit

II and IV. Within these layers the ratios of 90th to 10th percentiles are low, resulting in a better sorting (Kehl et al., 2014).

Comparing these results of the granulometric analyses with the samples in which the carbonate was previously destroyed (by means of HCl 10%), little change in the particle size distribution can be detected (**Supplementary Figure S1**). The peak within Unit V is also verified. Only the samples within the sterile Unit VI show a slightly different behavior to the samples which were exclusively sampled with H_2O_2. Nevertheless, the main grainsize fraction remains sandy medium silt to sandy coarse silt.

Using VIS spectrophotometer to analyze the color of the dried and powdered sediment, significant color changes in the upper part of the sediment column are obvious. Shades of dark brown alternate with lighter gray colors and more intense red-brown colors. In **Figure 4** the lighter shades of Units II and IV are particularly prominent, which are accompanied by an increase in the L* values and a decrease in the a* and b* values (**Supplementary Figure S1**). The a* value peaks in Unit V and in the upper part of Unit III, which could also be observed in the field. Especially this part of Unit III appeared brick-red under the prevailing lighting conditions inside the excavation trench. The values of the redness index (RI) corresponds to the a* values and the iron content within the sedimentary sequence. It also illustrates the decrease of iron oxides within Unit VI.

FIGURE 5 | Sedimentological and geochemical properties of the profile F35: carbon content (TC and TOC); element trends (Fe_2O_3, Fe, K, P, Mn); element ratios (Al/Ti, K/Rb), calculated index of alteration (CIA).

Magnetic susceptibility (MS) was measured in order to identify signals of human induced burning. The peak values are found in Unit III, V and VII, where archaeological finds are concentrated. Also, the darker color of the sediment, e.g., degreased values of the L^* curve, correspond to higher magnetic susceptibility. The minimum values are found in Unit II, IV, VI and the lower part of Unit III.

The carbonate content in the samples varies strongly in the upper part of the profile and peaks within Units I, III and especially in Unit V. Within the lower section of the profile the amount remains relatively constant at around 0.5%. The measured TOC content shows minor deviations from the TC curve, thus it can be expected that little or no carbonate was precipitated after sedimentation (**Figure 5**).
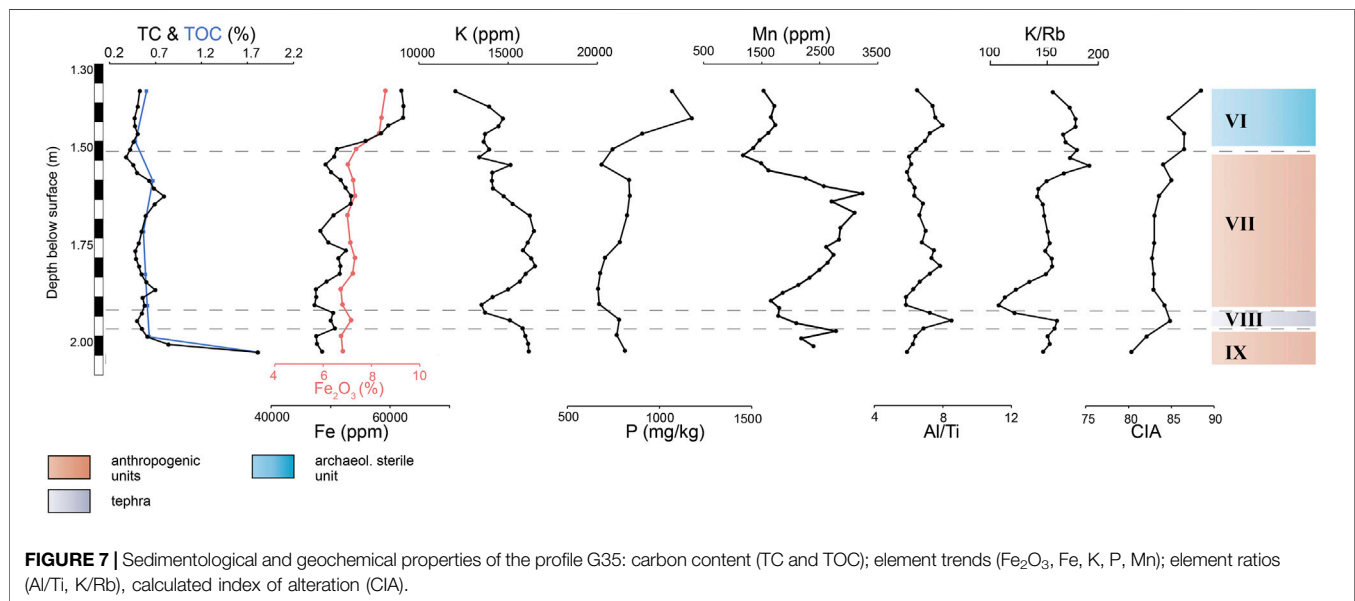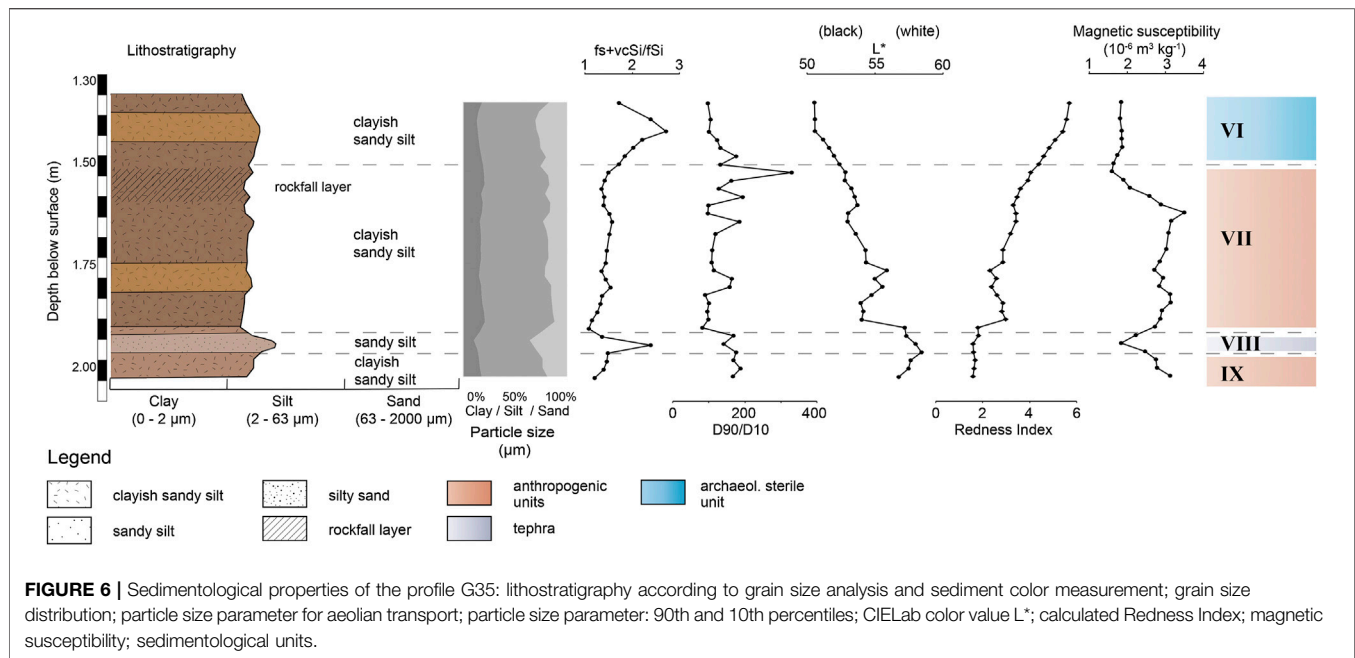
An XRF analysis allows the detection of several counted elements present in the samples, but only a selection of the results is considered in this study. **Figure 5** illustrates that Iron (Fe), one of the most common trace elements on earth, shows relatively low values in the upper profile part. With the beginning of the Unit VI the Fe counts and the Iron (III) oxide (Fe_2O_3) percentage amount rise. The elements aluminum (Al) and titanium (Ti), often used as indicators for stronger weathering, show a similar course with enrichment in the sterile clayish Unit VI (**Supplementary Figure S1**). Diametrical to this are the curves of mobile alkali metal potassium (K), rubidium (Rb) and halogen chlorine (Cl), which are abruptly depleted in Unit VI. Peak values are found

in Units II, IV and in the middle part of Unit III. The light element Silica (Si) is enriched within the same units in the upper part of the profile. The values of calcium (Ca), strontium (Sr), phosphorus (P) and manganese (Mn) are elevated in the Units III, V and VII which represent anthropogenic layers (**Figure 5**).

Selected element ratios, as Al/Ti and Fe/Al indicate major changes in the source areas of the deposits. Following the graphs in **Figure 5** and **Supplementary Figure S3** the Units II, IV and the middle of Unit III that can be characterized as volcanic ash with higher ratios of Al/Ti and Fe/Al. In contrast, Unit VI differs by very low values. According to the ratios of mobile to less mobile elements, e.g., between K/Ti and K/Rb, the lower section of the profile reflects changes into a regime with increased weathering (Brown, 2011; Arnaud et al., 2012; Kehl et al., 2014; Kehl et al., 2016). The calculated chemical index of alteration (CIA) peaks in the lower Unit VI of the profile. The resulting graph of the Mn/Fe ratio in **Supplementary Figure S3** shows an increase in the anthropogenic Units I, III and V.

Profile G35

The lower examined section in square G35 consists of the sedimentological Units VI to IX. The granulometric analyses and statistical analyses points to a tri- and polymodal grain size distribution as well as a very poor sorting throughout all the samples. (Sandy) medium silt is the dominant mean fraction within the whole sample column with variations of very fine sandy medium silt to medium and coarse silt. The exception

FIGURE 6 | Sedimentological properties of the profile G35: lithostratigraphy according to grain size analysis and sediment color measurement; grain size distribution; particle size parameter for aeolian transport; particle size parameter: 90th and 10th percentiles; CIELab color value L*; calculated Redness Index; magnetic susceptibility; sedimentological units.

FIGURE 7 | Sedimentological and geochemical properties of the profile G35: carbon content (TC and TOC); element trends (Fe_2O_3, Fe, K, P, Mn); element ratios (Al/Ti, K/Rb), calculated index of alteration (CIA).

are two peaks within Unit VI and Unit VIII where the grain size is slightly higher. In addition, there is an increased proportion of the grain sizes fine sand and coarse silt (40–125 μm) which can be associated to an aeolian origin (**Figure 6**) (Kehl et al., 2014). The samples with this specific grain size range also show low ratios of the 90th and 10th percentiles and therefore a higher sorting.

The analyses of the sediment color show insignificant changes from brown to light brown. With increasing depth, the luminance (L*) increases and the red tones (a*) decrease (**Supplementary Figure S2**). During the field work the lower sediment sequences were described as reddish due to the limited daylight inside the shelter and the high moisture of the sediment. Actually, the calculated redness index in **Figure 6** illustrates a slow decrease of the values with increasing depth, which are synchronous to the Fe and Fe_2O_3 values.

The magnetic susceptibility shows increased values in the upper part of Unit VII and in the lower most Unit IX that is an anthropogenic layer. The values peak in the settlement layers, but generally less pronounced as in the profile F35.

TABLE 1 | Radiocarbon ages for samples from Sodicho Rockshelter, arranged by archaeological excavation units.

Lab code	Excavation unit (square-quarter-level)	Specimen	S.Unit	Conventional^{14}C-date [BP]	Calibrated^{14}C age range (2σ) [cal BP] IntCal20.14c	Prob. (%)	δ^{13} (‰)	Sample depth [cm b.s.]
Beta-449167	F34-SW-02	Charcoal	I	250 + 30	**270–322**	56	−27.9	8
Beta-449166	F34-NW-02	Charcoal	I (pit)	350 + 30	**315–411**	59	−24.8	11
COL3149.1.1	F35-SW-06	Soot	III	1944 ± 46	**1,741–1,948**	93	−26.1	excl.
COL3150.1.1	F35-SW-07	Charcoal	III	1806 ± 42	**1,685–1,824**	59	−24.1	excl.
Beta-449168	F34-NW-10	Charcoal	III (pit)	2,130 + 30	**1,999–2,153**	88	−25.7	48
Beta-486041	G34-NW-11	Charcoal	V (hearth)	3,860 ± 30	**4,227–4,407**	84	−25.0	44
Beta-449169	G35-NE-15	Charcoal	V	3,920 ± 30	**4,242–4,424**	99	−26.4	56
COL3153.1.1	F35-SW-14	Charcoal	V	4,054 ± 45	**4,418–4,647**	88	−27.2	excl.
Beta-449170	G35-NE-18	Charcoal	V	4,060 + 30	**4,422–4,621**	92	−24.9	69
Beta-450067	F34-NE-18	Seed	V	4,190 + 30	**4,617–4,765**	74	−21.7	69
Beta-449171	G35-NE-19	Seed	V	4,130 + 30	**4,567–4,729**	64	−23.3	77
Beta-449175	G35-NE-20	Seed	V	4,160 + 30	**4,610–4,828**	94	−24.6	84
Beta-434190	G35-NE-23		VI	4,130 + 30	**4,567–4,729**	64	−25.9	excl.
Beta-449172	G35		VI	9,540 + 40	**10,695–10,897**	51	−22.3	150
Beta-449173	G35-NE-23	Charcoal	VII	11,620 ± 40	**13,401–13,521**	75	−22.1	excl.
Beta-481344	G35-SE-24	Charcoal	VII	12,560 ± 40	**14,812–15,122**	85	−25.1	159
Beta-523129	G35-NE-27	Org. Mat	VII	5,640 ± 30	**6,390–6,490**	78	−25.2	160
Beta-434191	G35-NE-28	Charcoal	VII	13,970 ± 50	**16,738–17,121**	100	−21.7	158
Beta-434192	G35-NE-28	Charcoal	VII	13,930 ± 50	**16,718–17,072**	100	−24.0	156
Beta-449174	G35-NE-28	Charcoal	VII	13,870 ± 50	**16,644–17,025**	100	−22.2	156
Beta-521542	F35-SE-26 B	Charcoal	VII	13,970 ± 50	**16,738–17,121**	100	−25.6	165
Beta-521541	F35-SE-26 a	Charcoal	VII	4,010 ± 30	**4,415–4,530**	99	−25.3	163
Beta-521539	F35-SE-27 a	Charcoal	VII	13,870 ± 40	**16,664–17,016**	100	−25.8	170
Beta-521540	F35-SE-27 B	Charcoal	VII	13,860 ± 50	**16,631–17,016**	100	−25.9	170
Beta-481345	G35-SE-31	Charcoal	VII	14,910 ± 50	**18,134–18,293**	100	−25.4	178
Beta-481347	G35-SE-37	Charcoal	IX	17,800 ± 60	**21,392–21,867**	100	−24.5	199
Beta-487731	G35-SE-37d	Sediment	IX	21,210 ± 70	**25,292–25,749**	100	−24.3	203
Beta-486039	G35-SE-37C	Charcoal	IX	22,360 ± 80	**26,396–26,960**	100	−24.7	203
Beta-521544	G35-SE-38 a	Charcoal	IX	22,350 ± 80	**26,392–26,953**	100	−24.2	204
Beta-521545	G35-SE-38 B	Charcoal	IX	22,510 ± 80	**26,452–27,107**	100	−26.2	206
Beta-521547	G35-SE-39 B	Charcoal	IX	22,450 ± 70	**26,433–27,029**	100	−25.5	206

Roman numbers indicate sedimentological unit. The bold numbers represent the calibrated ^{14}C age range (2σ) in cal BP. Samples Beta-434190 and Beta-449172 were taken from the archaeologically sterile layer. Red numbering indicates sample depth that where defined by the excavation unit, "excl." illustrates samples that were excluded from the depth model.

The measured carbonate content in the samples also represents the TOC content as in the samples of profile F35, since the pretreatment with HCl (10%) did not show any significant changes in the values. Thus, the carbonate content of the samples can be addressed as organic carbon. A post-depositional formation of inorganic carbon, such as gypsum or carbonates is therefore insignificant. The carbonate content is expressed in three extreme peaks within the Units VII and IX.
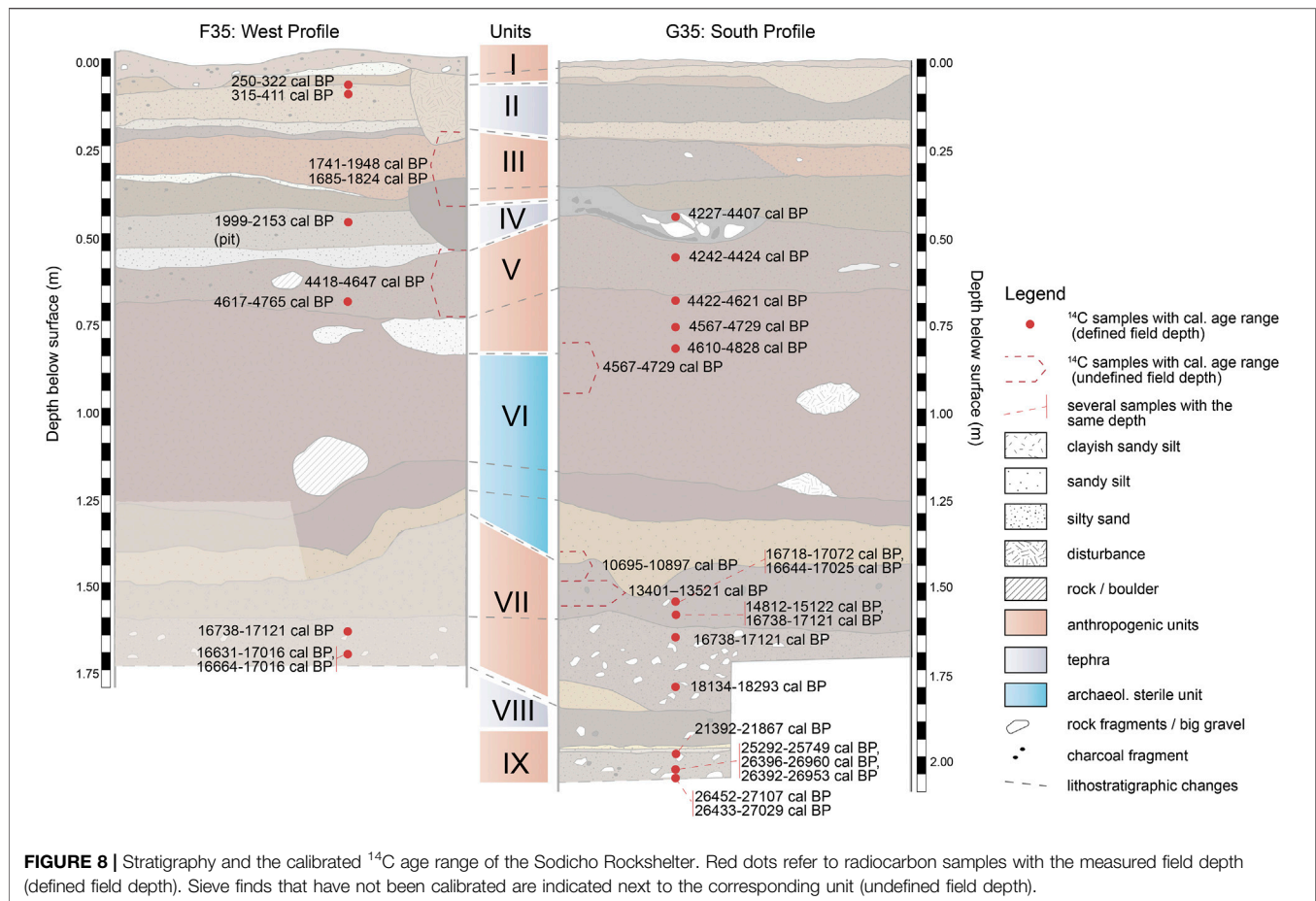
The resulting curves of Si and Ti show similarities especially in the increased values within the anthropogenic Units VII and IX. The lowest values are found in the Units VI and VIII (**Supplementary Figure S2**). Ca and Mn are increased in Unit VII and IX, that is comparable with the peak values of magnetic susceptibility within the cultural layers. Especially Mn is marked by higher values in Unit VII (**Figure 7**). Rb and strontium also share the same minimum as Ti within Unit VII, although the resulting curve differs in Unit IX with slightly increasing values. The values of K on the other hand show a different pattern with minimum values in Unit VIII. In contrast the P, Cl values peak in Unit IV sand IX, following the increasing grain size. The graph of Al does not show as pronounced

changes as in profile F35 but it displays a rising gradient of the values within the units with a higher mean grain size.

The ratios of Al/Ti and Fe/Al, that are often used to indicate changes in the source area of sediments during deposition (Kehl et al., 2014), show only slight variations within profile G35. In **Figure 7** and **Supplementary Figure S4** the low values of the ratios of K/Ti and K/Rb indicate a slightly increased influence of weathering on the deposits in Unit VII (Brown, 2011; Arnaud et al., 2012; Kehl et al., 2014; Kehl et al., 2016). These rather small changes can also be observed in the calculated CIA. As already observed in the profile F35, the Mn/Fe ratio is increased in the anthropogenic influenced layers VII and IX (**Supplementary Figure S4**).

Radiocarbon Chronology

According to the analyses, the stratigraphy can be roughly divided in five settlement phases, including the uppermost dated phase of recent times (**Table 1**). This proofs repeated occupation by humans since more than 20 thousand years. The radiocarbon samples originate predominantly from anthropogenically

FIGURE 8 | Stratigraphy and the calibrated ^{14}C age range of the Sodicho Rockshelter. Red dots refer to radiocarbon samples with the measured field depth (defined field depth). Sieve finds that have not been calibrated are indicated next to the corresponding unit (undefined field depth).

influenced layers (**Figure 8**), with the exception of samples Beta-434190, Beta-449172 and Beta-481345, which originate from archaeologically sterile layers. The samples Beta-523129 and Beta-521541 show comparably younger radiocarbon ages to the samples of the same depth, which probably indicates post-depositional displacement or inconsistencies in the sampling procedure.

A modifiable classical age depth model was generated with the help of the clam2.3.5 package in RStudio. The model uses a linear interpolation technique with calculated accumulation rates to illustrate the changing deposition processes within the rockshelter. In **Figure 9** the mentioned human settlement phases accumulated relatively fast. The intermitted archaeological sterile layers deposited comparably slow. Despite these similarities between the calculated ages and the age-depth model, several calibrated age ranges cannot be considered in the model, which are highlighted as "excl." (**Table 1**). This includes the sample COL3149.1.1, COL3150.1.1, COL3153.1.1, which were taken during the test excavations of 2015 when no total station was available to record the exact location of the samples. The samples Beta-434190 and Beta-449173 are sieve finds and had to be excluded as well, since an exact field depth could not be measured. Samples that have been included in the model but clearly show a significant age

deviation are marked as outliers. In **Figure 9**, a "plateau" is shown between 10.8 and 17 ka, which is due to the fact that the sample Beta-481344 is considered an outlier. If the Beta-481344 was included in the model, two other samples (Beta-449174 and Beta-434192) would have to be excluded to prevent a reverse chronology (**Figure 9**). This illustrates how variable the sediment deposition is within Sodicho Rockshelter and how difficult it is to develop a reliable model.

Archaeological Finds

The analysis of the archaeological finds is still ongoing and only preliminary results based on the analysis of artifacts from square F35 & G35 can be presented in this chapter. The preservation conditions for bones are extremely bad, due to the volcanic and moist environment of the shelter. The acid character of the sediments in combination with leakage water caused the destruction of any bones older than some hundred years. Pottery is also restricted to the recent surface layer and the youngest Stone Age occupation. This confirms the general picture of a late appearance of pottery in the southwestern Ethiopian Highlands around 2000 years ago (Gutherz et al., 2002; Hildebrand and Brandt, 2010; Schepers et al., 2020).

In all other cultural layers are stone artifacts the only cultural remains. The broad division of the stone artifact assemblages

FIGURE 9 | Age-depth model with sediment units and probability distribution of the calibrated radiocarbon ages (red box plot). Possible course of a model that includes sample Beta-483144 is indicated by a red dashed line. Gray circles indicate outlier and samples that are discussed in the manuscript.
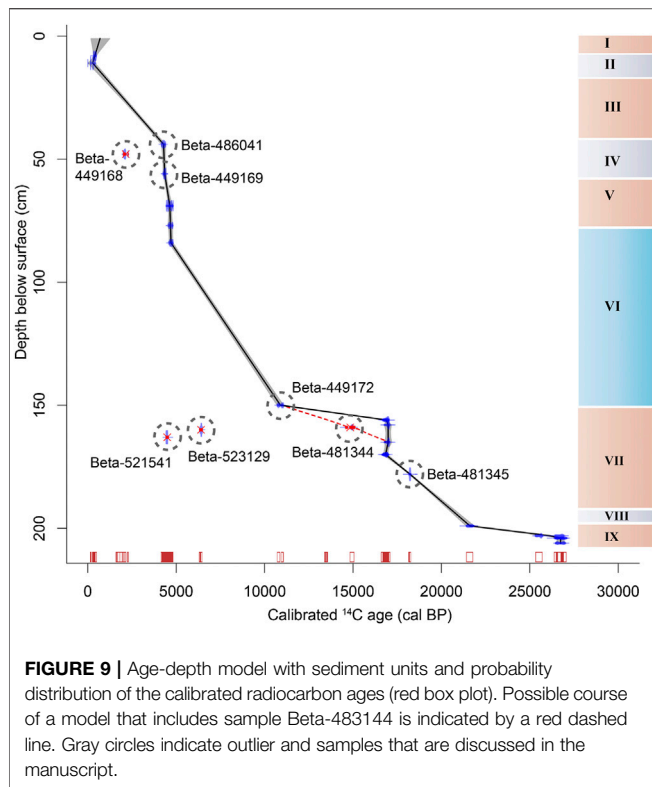
reflects the general sedimentological differentiation of an upper sediment package, which is separated by a sterile, reddish-brown deposit (Unit VI) from a basal sediment package. Chronologically, this division can be correlated with the Late Holocene and the Late Pleistocene, separated by a Middle to Early Holocene occupational gap.

Raw material for the production of stone tools is in all assemblages almost exclusively obsidian. First microprobe analysis results verify the exploitation of two local sources and of the large Bantuu outcrop, which was also used by the occupants of the rockshelter Mochena Borago. In addition, several up to now unknown raw-material sources have been used (pers. communication B. Nash). The two cultural layers in the upper part of the stratigraphy (Unit III and Unite V) are both characterized by microlithic stone tools, mainly backed tools, which are type forms of the African microlithic Later Stone Age (LSA). The main difference between the two assemblages is the number of artifacts. Only 69 pieces (without chips) from the upper LSA assemblage in square F35 stand in contrast to 531 pieces from the older LSA assemblage. The small number of stone artifacts of the upper LSA assemblage, which dates between ~1800 and ~2,100 cal BP, accounts for the low number of retouched tools. Despite two fragments of backed microliths that cannot be further classified, two segments are the only characteristic type-forms. The older assemblage, which dates between ~4,300 and ~4,800 cal BP, comprised 11 segments (**Figure 10**), seven micro-points and six double micro-points (following the definition of type-forms in Schepers et al., 2020). Single pieces are one scraper, one backed point and one drill.

However, the percentage of retouched stone tools in comparison to the total number of stone artifacts is in both assemblages similar. The greater variation in type-forms of the older microlithic assemblage might be simply due to the higher total number of artifacts. Regarding the small sample size coming from a very restricted area of the shelter, further analysis has to verify, if the different spectrum of tools reflects any cultural or functional distinctions and if the number of finds reflects different settlement intensities.

A sediment package without any cultural remains (Unit VI) represents an occupational gap between these younger, microlithic assemblages and the Late Pleistocene assemblages. Repeated occupation of the shelter is testified between ~27,000 and ~13,500 cal BP. Preliminary analysis of the lithic assemblages shows a surprising uniformity of the stone artifacts. Obsidian is still the dominant raw-material for the production of stone tools, but also cryptocristalline silices were used in small numbers. All assemblages are dominated by the production of bladelets and the analyzed sample completely lacks any retouched tools (**Figure 11**). Settlement phases dating around 17 to 15 ka cal BP and 27 to 22 ka cal BP coincide with the arid or rather hyper-arid climatic phases of the Heinrich event 1 and 2 (H1, H2) (Hemming, 2004) and the Last Glacial Maximum (Mark and Osmaton, 2008).

DISCUSSION

Interpretation of Multiproxy Analyses
Our sedimentological and geochemical results revealed major changes of the sediment sources and indicate a combination of different geogenic and anthropogenic processes that influenced the deposits in the Sodicho Rockshelter. Our data revealed that the sedimentological units preserved within Sodicho Rockshelter accumulated in different depositional environments. Based on field observation and analyses we distinguished a total of nine sedimentological units, which can be grouped in four sediment facies:

Autochthonous geogenic deposits are mainly characterized by trachytic clasts and boulders, that could derive most likely from the rockshelter walls and the roof itself. This type of deposit is omnipresent in almost all sediment units. A rockfall layer located in the upper part of the Unit VII, right below the sterile Unit VI, consists of trachytic boulders with a maximum diameter of up to 70 cm (**Figure 4**). The upward facing surface of the boulders is rounded. This indicates that the boulders were not rapidly covered by sediment and persistent weathering dissolved the fine feldspar matrix.

Allochthonous geogenic deposits predominantly consist of well sorted volcanic tephra and ash, which were ejected during past volcanic eruptions in the region and deposited in the shelter by aeolian transport. These Units II, IV and VI are easily identifiable as thicker, light color sediment layers or lenses, with an increased mean grain size. The grainsize analyses revealed low ratios of the 90th and 10th percentiles and a higher amount of particle with the grain size that can be associated to an aeolian transport. These results and the field observation indicate major changes in sediment origin during
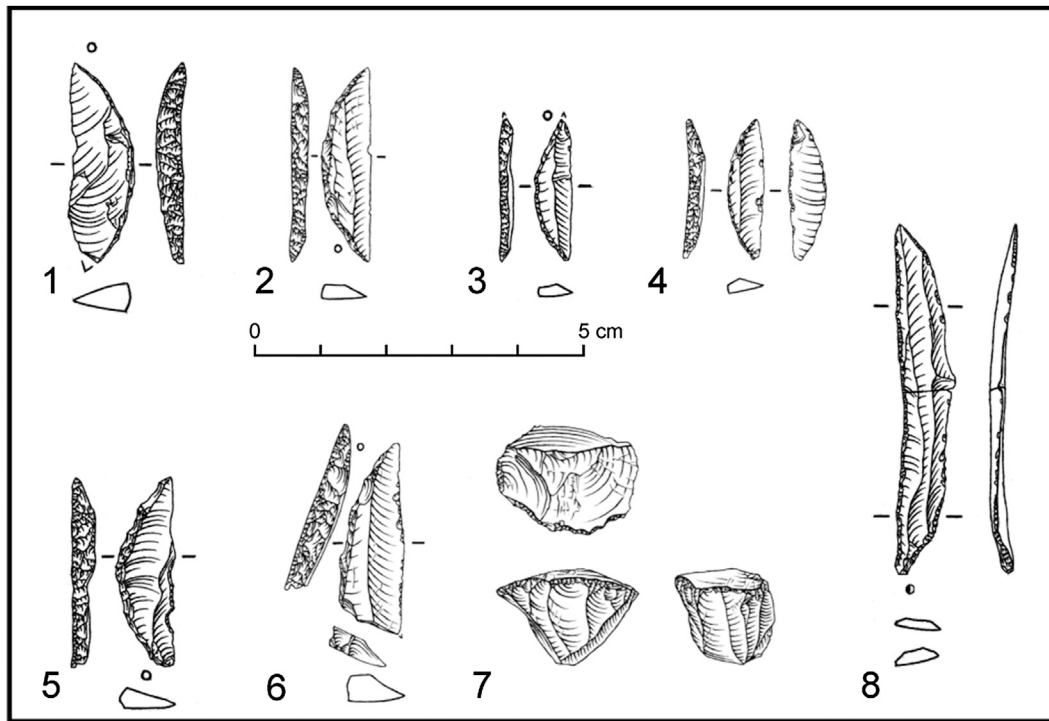
FIGURE 10 | Microlithic LSA lithics: Segments (1–5), backed point (6), prismatic bladelet core (7), broken bladelet with use-wear (8).
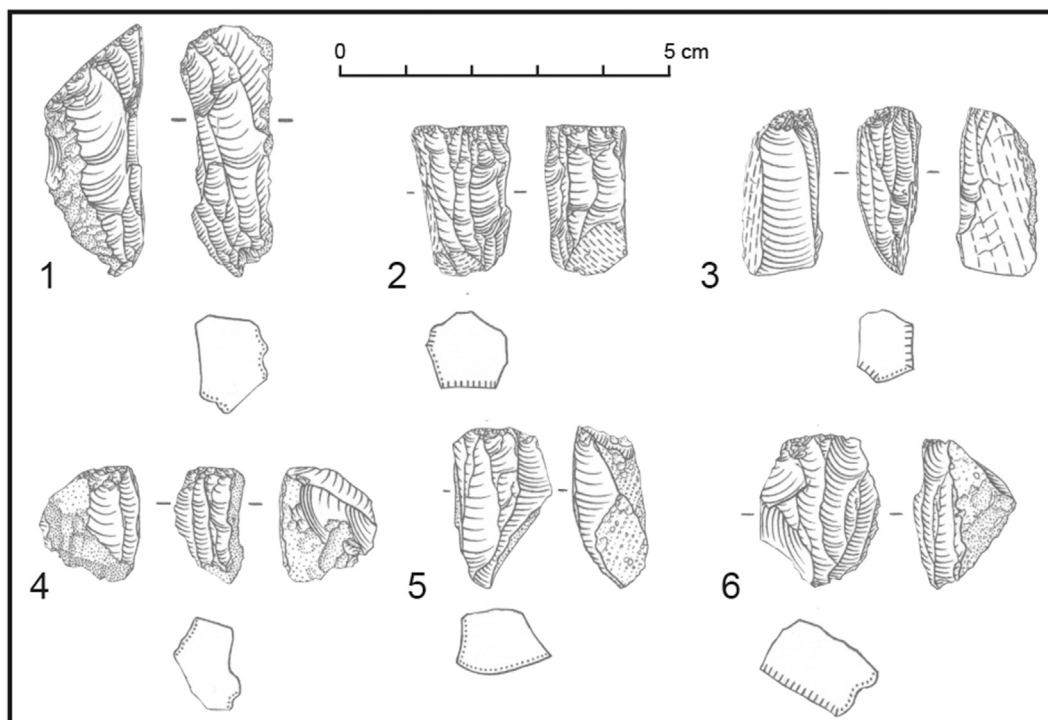

FIGURE 11 | Late Pleistocene lithics: Bladelet cores (1–6).

deposition with the highest aeolian input in Units II, IV, and partly in III. Geochemical analyses point to a potassium and chlorine enriched felsic tephra, that is distinguishable from the surrounding sediment. This geochemical fingerprint allows the identification of altered volcanic tephra within samples, as identified in Unit VI and VIII. The source volcanos of the tephra remain undefined, even though we identified the geochemical composition. It can be assumed that this type of allochthonous geogenic deposits of volcanic origin were deposited relatively abrupt, which is shown by the sharp boundaries to lower deposits.

Mixed autochthonous and allochthonous geogenic deposits are the result of weathering of the trachytic rock and water percolation through the sediment. This type is common in the sterile Unit VI, that differs from all the other sediment units in both sample columns. The poor sorting in these deposits indicate polygenic sediment origins. The high CIA index as well as low K/Ti, K/Rb values refer to increased (Kehl et al., 2014). The reddish-brown deposits are characterized by an increased clay content and peaks in the redness index that correspond with a higher Fe_2O_3 content (**Figure 5**). Particularly noticeable is the decrease in magnetic susceptibility and most other geochemical proxies. Nevertheless, Ti and Al content are increased since they are often bound to clay (Okrusch and Matthes, 2010). Based on its high Fe_2O_3, Ti and AL content, we argue that Unit VI originated from the weathering of the local bedrock in a moist environment, leading to the formation of authigenic clay minerals. Alternatively, the increased clay content and the different geochemical composition of this sediment could be the result of fine-grained soil material that was washed in the site through fissures in the ceiling of the rockshelter.

Anthropogenic deposits are identifiable by the concentration of archaeological finds, such as obsidian artifacts and charcoal from hearths, as observed in Units I, III, V, VII and IX. Moreover, the deposits have a certain sedimentological and geochemical fingerprint that is characterized by a poor sorting, high values of magnetic susceptibility and an increased content of Mn, P and TOC (**Figure 4–7**). Manganese and Phosphorous are released into the soil by the decay of deposited organic matter or inorganic compounds, as in phosphate minerals, that accumulate at the site by human occupation (Holliday and Gartner, 2007; Karkanas, 2017). Furthermore, the high percentage of TOC in Unit VII and IX can perhaps be explained by higher weathering of the lower levels of the stratigraphy and therefore the decomposing of the organic matter. The high values of the magnetic susceptibility most certainly derived from thermally alteration of the sedimentary substrate, due to burning activity. Chemical changes of magnetic minerals induce the development of ferrimagnetic mineral, such as maghemite that increases the magnetizability of the sediment (Le Borgne, 1955; Herrejón Lagunilla et al., 2019). Furthermore, manganese shows paramagnetic properties, which contributes to the relatively high ratios of magnetic susceptibility in the cultural layers. This means that randomly distributed magnetic dipoles interact with the external field of the magnetic susceptibility measurement, which orients the dipoles in one field direction, and amplifying the whole field (Ivers-Tiffée and von Münch,

2007). The Mn/Fe ratio is increased in the anthropogenic Units I, III and V (**Supplementary Figure S3**), suggesting increased manganese content under redox conditions in the upper part of the stratigraphy.

Although the sedimentological and elemental fingerprints show clear signs for human occupation, we cannot exclude that these layers underwent diagenetic processes such as dissolution or oxidation. This can bias results about environmental condition during human occupations in the shelter. By comparing the geochemical data of profile F35 with profile G35, it is noticeable that the values of the sedimentological and geochemical graphs of the basal sediment levels below the sterile unit are not as pronounced, which indicates stronger alteration. This may be caused by a higher influence of water infiltration during the deposition of the sterile layer that can be dated to the AHP (~15–5 ka BP) and a possible post depositional alteration.

Chronology and Human Occupation at the Rockshelter

We assigned the multiproxy results to the radiometric ages and via the age-depth model in order to understand site formation processes and to correlate them with the chronological succession of the cultural layer. Following the mentioned sedimentological and geochemical results we can distinguish nine sedimentological units, comprising of both natural and anthropogenic accumulations (**Figure 8**). The following chronological phases of human occupation are described in stratigraphic order. It is important to note that the calculated age-depth model cannot reflect the complete depositional conditions and their variations in the Sodicho Rockshelter, as these processes vary within the different excavation quadrants. The model is intended as a simplification to illustrate phases of human settlement.

Mount Sodicho is probably one of the silicic domes associated to the Wagebeta Caldera Complex that developed 3.6- to 4.2 Ma ago (WoldeGabriel et al., 1990; WoldeGabriel et al., 1992). The exact time for the formation of the Sodicho Rockshelter and the beginning of sediment deposition is not yet clear. Therefore, further investigations and excavations down to the bedrock are needed. The rockshelter increased in size as time progressed due to solution of silica in the trachytic rock by water that flowed in through fissures and cracks in the weathered rock shelter roof, which are still visible today.

As discussed above, the lowermost investigated Unit IX with an approximate age range of about ~27 to 22 ka cal PB represents an anthropogenic layer (**Figure 8**). Charcoal fragments and lithic artifacts as well as the characteristic anthropogenic deposits with increased magnetic susceptibility, higher manganese and phosphorus content indicate human occupation. The base of this layer has not been reached yet. The excavation unit GE35-SE-37 is represented only by a single date (Beta-481347) in the age-depth model, although two other samples (Beta-487731, Beta-486039) derive from this level (**Figure 9**). Their different age can be explained by the presence of a coarser-grained and lighter colored band in Unit VIII, with increased values of Al/Ti, which indicates a variation of the sediment source. The influence of post-depositional processes such as bioturbation cannot

be excluded, which has to be a focus of future micromorphological investigations.

Sediment Unit IX is covered by a brownish layer, representing a distinct anthropogenic unit (VII), which lies below the archaeological sterile unit. The lower part of the unit consists of a yellow brownish sediment with intermixed cultural findings. One radiocarbon sample that was collected from this section dates between 21,392 and 21,867 cal BP. The following settlement phase covers a period of about 17 to 15 ka cal BP. All radiocarbon samples were taken from sediment in-between and below the big trachytic boulders of the rockfall layer. Chronologically, the trachytic rock fall layer in the upper part of the unit cannot be assigned, as no datable material has been preserved directly above this layer. At the moment it is not possible to determine whether the collapse of the roof caused the end of this occupation phases or if the humans had already left the rockshelter. The stone artifact distribution in between and below the boulders points to a severe disturbance of the accumulated anthropogenic material. Another question is whether the larger rocks at the entrance of the rockshelter collapsed at the same time as the trachytic rocks in Unit VII, or if this was a different event. The absence of trachytic boulders in higher strata of the stratigraphy speaks for a simultaneous collapse of the rocks. Future analyses below the large rocks, blocking the entrance, could provide information about this. It can be assumed that the whole sedimentological unit has undergone post-depositional processes that let to disturbances and influenced the expression of some geochemical indicators. A possible influence of pedogenetic processes and temporary absence of human impact can be explained by the inconsistency of the magnetic susceptibility and the K/Rb ratio (Kehl et al., 2014). This indicates post-depositional disturbances and a possible displacement of radiocarbon samples. With this assumption in mind the two outliers (Beta-523129, Beta-521541) of this cultural phase, can be excluded from the model.

The following clayish Unit VI provides a unique indication for the prolonged absence of humans. Chronostratigraphically, this unit can be dated by one radiocarbon date (Beta-449172), that originates from the base of the unit, and by the dates of the cultural layer below and above it. Based on this, the dates of ~15 and 4.7 ka are the maximum, respectively minimum age of the deposition. This period can be assigned to the Early Holocene African Humid Period (Foerster et al., 2012; Foerster et al., 2015; Hildebrand et al., 2019). An exact dating of the deposits is not possible due to the lack of datable material within Unit VI (**Figure 8**). The duration of the deposition is unclear and it might have been a slow process over a long period or a rapid event. It can be assumed that there must have been fluctuations during the deposition. This is verified by the variations in the degree of sorting and by the distinctive yellowish, silty layer in the lower part of the unit.

The end of the archaeologically sterile Unit VI and thus the beginning of the anthropogenic unit V is verified by the presence of obsidian tools and charcoal, as well as by the abrupt change in sedimentological and geochemical features. In particular, the increased values of magnetic susceptibility, TOC, as well as the increase in manganese and phosphorus mark an intense re-occupation of the shelter by humans. Seed and charcoal samples date to an age range of about ~4.7–4.3 ka cal BP. Again, the accumulation rate of the anthropogenic impacted deposits in Unit V is higher than in the case of exclusively geogenic induced deposits in the Sodicho Rockshelter. Considering the sampling depth of the radiocarbon samples, the anthropogenic accumulations reach up to a field depth of 0.45 m. However, the samples Beta-486041 and Beta-449169, collected in excavation square G, are at the same depth as the sterile tephra of Unit IV in square F35, which is not visible in square G. These tephra layers can be geochemically identified by the coarser grain size, the increased potassium (K) amount and the maximum values of the Al/Ti proxies, which indicates a change in the sediment source (Kehl et al., 2014). In addition, sweeping and raking-out the surface may have been involved, as has already been observed in micromorphological studies at South African sites, like Sibudu Cave and Diepkloof Rock Shelter (Goldberg et al., 2009; Texier et al., 2010).

The radiocarbon sample Beta-449168 is marked as an outlier in the age-depth model because it was taken from a pit in excavation unit F34-NW-10 (**Figure 9**). Stratigraphically the sample is situated above sample Beta-486041 in Unit III (**Table 1**). This age discrepancy is the result of mixing and relocation of the sediment in the pit (Ossendorf et al., 2019). Nevertheless, the dated sample represents the anthropogenic Unit III, which is supported by cultural material and an increase in TOC and of manganese.

On the basis of the geochemical proxies alone, it can be assumed that the human occupation of the rockshelter was more pronounced in the periods above the sterile layer than in the stratigraphically older units. However, it should be pointed out that the proxies at the bottom of the sterile layer show weaker trends and were probably influenced by weathering. Considering the small size of the excavation trench, the artifact density might simply reflect differences in the spatial use of the shelter over time and is therefore an incidental result that cannot be considered as an indicator for settlement intensity.

Regional Paleoenvironmental Implications

The sedimentological results indicate changes in the depositional conditions over time. As discussed above, some of the results, e.g., archaeological finds, magnetic susceptibility and the Mn content show clear signs of human impact. By plotting elemental ratios against the calculated age-depth model, it is possible to model these first results in relation to regional paleoenvironmental changes during the last 27 kilo years (**Figure 12**), covering periods like the Last Glacial Maximum (LGM, 21 ± 2 ka) and the Early Holocene African Humid Period (AHP, ~15–5 ka). For the paleoenvironmental comparison we consider archaeological and sedimentological information from the rockshelter Mochena Borago, and paleoclimatic records from lacustrine sediments in Ethiopia. With our own data we observe local environmental fluctuations in sediment sources or weathering intensity caused by shifts in moisture availability.
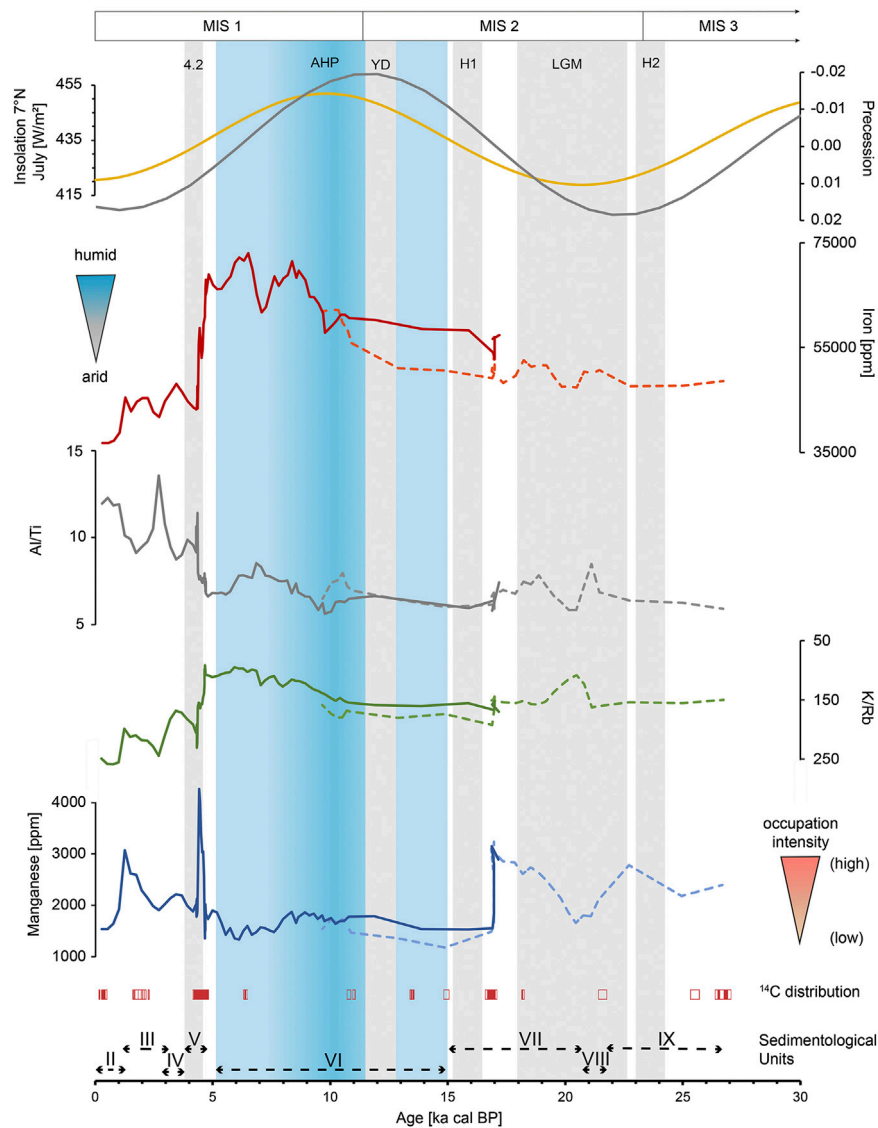
FIGURE 12 | Comparison of geochemical records with paleo-climate records (continous line = results F35, dotted line = results G35. Plotted from top to bottom: insolation variations 21st July, 7°N (Laskar et al., 2004); orbital precession (Laskar et al., 2004); Fe content with associated blue triangle shaped symbol (climate); K/Rb ratio (note reverse scale); Al/Ti; Mn content with associated orange triangle shaped symbol (occupation intensity); gray bars illustrate climatic dry events (4.2 event, Younger Dryas, Heinrich 1, Heinrich 2, Late Glacial Maximum); blue bar refers to African Humid Period; Reddish box plots illustrate ^{14}C distribution of Sodicho Rockshelter; roman numbers and bars illustrate sedimentological units.

Phase 3: Unit VII–IX, ~27–15 Ka

The short distance of about 40 km to Mochena Borago provides a suitable basis for a local comparison of the past conditions. Chronologically, the currently excavated and dated cultural layers from Sodicho cannot be connected to the Late Pleistocene deposits of Mochena Borago, since layers from this period have not been excavated yet. Nevertheless, we see similarities in the changes of the lithostratigraphic sequences. The basal Pleistocene deposits of the stratigraphy of Mochena Borago offers one of the most complete records from the timeframe of 60–30 ka in Eastern Africa. The main trench at Mochena Borago revealed three major lithostratigraphic units

that preserved cultural remains dated between 36 and >50 ka (Brandt et al., 2017). The complex stratigraphy developed by multiphase, polygenetic accumulations of geogenic deposits, e.g., fluvial activities, volcanic eruptions, and anthropogenic depositional processes (Brandt et al., 2017). Several erosional activities resulted in a chronostratigraphic gap from ~36 to ~8 ka cal BP, erasing sedimentological history and possible cultural evidence until the Holocene (Brandt et al., 2012; Brandt et al., 2017). Although this archaeological and stratigraphic gap was recognized at other East African sites as well, e.g., Ziway-Shala basin and Goda Buticha (Tribolo et al., 2017), it is not found in Sodicho. In **Figure 12** the Mn record and the ^{14}C dates illustrate

two anthropogenic Units IX and VII that preserved cultural material ranging from ~27 to ~16 ka cal BP. This makes Sodicho Rockshelter the first site in Ethiopia that partially reduces the chronostratigraphic gap. The two anthropogenic units partly cover the global short-term Heinrich event 2 (H2) and the prolonged high-latitude LGM with a decrease of the Mn values around 21 ka (**Figure 12**). On a regional level, both time ranges are pronounced dry and cold phases, that can be tracked by a drop in the K record of the Chew Bahir basin core (Foerster et al., 2012). In contrast to the geoarchaeological evidence from Mochena Borago indicating that prehistoric humans frequented the rockshelter during more humid conditions (Vogelsang and Wendt, 2018), the sedimentological and archaeological results at Sodicho point to multiple occupations during humid and arid periods. In fact, Sodicho is the first evidence for the use of highlands as a refugium during times of severe environmental stress in the lowlands. In the Rift Valley, human occupation is not traceable during Late Pleistocene arid phases, even not in the surroundings of lakes, such as the Ziway-Shalla Basin (Bon et al., 2013). Thus, highlands might have been the only retreats. Paleoclimate simulations indicate higher annual precipitation in the Ethiopian highlands during arid phases than in lower elevated regions in Ethiopia, and suggest that these regions were part of a warm and temperate savanna and remained covered by low growing vegetations and scrubs during the glacial aridity of the LGM (Basell, 2008; Willmes et al., 2017). Residual water in the highlands could have attracted animals and humans (Basell, 2008). The Mn value of Unit VII peaks around ~17 ka cal BP, followed by a rather extreme drop of the values, which was not evident in the raw data of the geochemical analyses of the stratigraphy (**Figure 7**). This indicates the end of the cultural settlement phase. At the same time the Fe values show a rather gradual change to more humid conditions. The rapid changes of the records can be explained by the calculated sediment rate of the age model, which is increased in this section. In addition, post-depositional processes, the rockfall event of Unit VII, and the human impact has to be considered. A further explanation is the sample Beta-481344 (14,812–15,122 cal BP), which was marked as an outlier in the calculated age depth model. When this dating would have been included in the age-depth model, the geochemical data does not show such a strong trend around 17 ka (**Supplementary Figure S5**). Nevertheless, the geochemical values would steadily decrease from 17 ka. Another possible explanation are stepwise abrupt changes to increasing precipitation. This observation is also preserved in the Chew Bahir basin record between ~19 and 15 ka, and further paleoclimatic records on the northern African continent (for detailed descriptions and references to these records, see Foerster et al., 2012). Overall, our geochemical data from this period around 17 to ~15 ka cal BP should be regarded with caution, since the age data are influenced by the plateau in the ag-depth model (**Supplementary Figure S5**).

Phase 2: Unit VI, ~15–4.7 ka

As mentioned before in **Figure 12**, a phase of prolonged human absence correlates with a shift to more intense moisture, expressed in low Mn content and higher Fe content. The overall moist signal is

recorded between a maximum age of ~17 ka cal BP and a minimum age of ~4.7 ka cal BP. Although Fe_2O_3 record has a comparable trend as Fe (**Figure 5**), the graph of Fe was chosen, due to the higher sample density and the more precise detection of fluctuations. This increased Fe trend, enhanced input of clay minerals and the lower K/Rb ratio corresponds to intensive weathering influence (**Figure 5**). As mentioned before this phase is known as the Early Holocene African Humid Period, that occurred during low orbital precession and associated higher insolation values (Laskar et al., 2004). Comparable conditions were observed in the increasing trend of the K record of the Chew Bahir basin (Foerster et al., 2012; Foerster et al., 2015). Our geochemical results in **Figure 12** show a gradual increase in humid conditions. In contrast, drier intervals like the Heinrich event 1 (H1, ~16 ka) and the Younger Dryas (YD, ~12 ka) are not visible in our geochemical record. This might be caused by one outlier sample that had to be excluded from our age model (see *Chronology and Human Occupation at the Rockshelter*). Nevertheless, a slight drop at 9.8 and 7 ka cal BP in the Fe values within the profile of F35 can be identified. These shifts can be explained by local changes in the sediment source region, as indicated by the fluctuations in the Al/Ti ratio. These intrusions correlate with a dry interval of 9.8–9.1 ka and a large-scale drought of around 7 ka observed at various sites throughout East Africa (Foerster et al., 2012). It is still unclear why the humans abandoned the rock shelter during the African Humid Period. Possibly the large lakes in the lowlands and Rift Valley offered preferred and easily accessible resources and the amount of energy needed to obtain food may have been lower there (Bon et al., 2013). Moreover, it can be assumed that the intense precipitation led to the formation of an extremely dense vegetation coverage, which impeded humans to live at the mountains slopes and use the highland ecosystems.

The termination of the AHP is a subject of current scientific discussions. These include the assumption of a slow gradual change to drier conditions (Kröpelin et al., 2008; Foerster et al., 2012) or a rather fast and relatively abrupt transition, which was also identified in several records, as according to water level reconstruction for the Turkana basin (Garcin et al., 2012). Furthermore, the role of humans as potential drivers for the end of the AHP is debated (Wright, 2017). These fundamental discussions go beyond the scope of this study that is based on a local data set. Regarding our analysis, after a maximum value of Fe around 6.5 ka cal BP a further weaker peak (4.8 ka cal BP) is followed by an abrupt drop in values, pointing to rather arid conditions. This abrupt change can also be seen in the other graphs of our figure. However, this is not an indication of the pace of termination of the AHP, since the sediment deposits at Sodicho are influenced by post-depositional processes. Furthermore, the deposition conditions in rockshelter settings are often somewhat more discontinuous, in comparison to other terrestrial or lacustrine deposits.

Phase 1: Unit V–I, ~ 4.7–0 ka

With the rapid decrease of the Fe values, the anthropogenic influenced Unit V emerges. Geochemically this can be clearly identified by increased MS and Mn values around 4.4 ka. This settlement phase and the associated deposition processes may have disturbed the sediment of the former walking horizon and thus partly explain the strong fluctuating Fe values. The dating of this cultural layer is of interest with regard to global climatic events, as it may cover

a time range that correlates with the so-called 4.2 ka event. This hyperarid event was mainly investigated in the Mediterranean (Kaniewski et al., 2018) or Chinese region (Xiao et al., 2018). Furthermore, a lacustrine record from Abhe Lake in northern Ethiopia indicates a drastic drop in lake levels between 4.5 and 3.7 ka, with an increase in aeolian accumulations indicating a drier climate (Khalidi et al., 2020). This could further confirm that humans lived in the Sodicho Rockshelter during arid periods with more favorable conditions in the montane forests (Hildebrand et al., 2019).

The tephra layers separating sedimentological Units I, III and V in excavation square F35 represent again a purely geogenic deposit and thus a temporary absence of humans within the rockshelter. The question whether humans were forced to abandon the site due to the volcanic eruptions and the consequential temporary environmental changes in the area cannot be answered on the base of the present results. Based on archaeological and chronological analyses at Mochena Borago, it is assumed that humans were influenced by rapid shifts in local or even regional environment that may have made it impossible to stay in the area (Brandt et al., 2012). The graphs in **Figures 4**, **6** of the sedimentological and geochemical analyses show that the deposition of the pyroclastic material occurred rapidly. Given the alternating tephra and cultural layers of the Sodicho stratigraphy, we can assume similar rapid changes influencing the surrounding landscape and the humans. In contrast we observe a rather slow change between Unit VII and the archaeologically sterile Unit VI. The geochemical analyses (slow decrease of MS and Mn content) may indicate that humans had already left the rockshelter.

CONCLUSION

The sediment record of Sodicho Rockshelter contains a 27 ka record of repeated human occupation and local paleoenvironmental proxies. The study presents a first stratigraphic and chronological framework for the Sodicho Rockshelter that is an important new site for studying prehistoric settlement in East Africa during critical time frames, such as the Last Glacial Maximum (LGM, ~ 21 ± 2 ka) or the African Humid Period (AHP, ~ 15–5 ka). Four sediment agents and the resulting site formation processes are identified. Purely geogenic accumulations differ significantly from anthropogenic induced deposits in terms of grain size distribution, sediment color and geochemical composition of the sediment. It is possible to indicate a higher intensity of human settlement phases during Unit V, according to the preliminary analyses of the lithic material, the results of magnetic susceptibility, and the content of Manganese and Phosphor. Archaeological sterile layers are identified with the help of sudden grain size variations and elemental ratios, like Al/Ti and K/Rb. These illustrate the deposition of volcanic fallout, changes of weathering intensity and shifts of major sediment sources. In particular, the Fe content reflects an increase in weathering caused by humid conditions between ~17 and 4.7 ka cal BP. Furthermore, the values also indicate short-term dry spells that may correlate with dated dry intervals of climatic records from the Chew Bahir basin, situated about 300 km southwest of the rockshelter but affected by the climatic

conditions of the southwestern highlands. In total, our results verify human occupation in the highlands during humid and arid phases in the last 27 ka. This underlines the assumption that the highlands might have been used as part of larger settlement areas during times of favorable climatic conditions, but also as retreat under arid environmental conditions. However, a distinctive settlement gap is detected during the humid conditions of the AHP. Further excavations and investigations are needed to verify these first preliminary hypotheses. These would include micromorphological observations and the evaluation of phytoliths, which could offer a closer look into the microstratigraphical development of the site and the local paleo-vegetation. Nevertheless, the sediment record of the Sodicho Rockshelter reflects local environmental changes that correspond to the records of the Chew Bahir basin and to superregional climatic shifts. The sedimentological and archaeological records of Sodicho Rockshelter have the potential to be correlated to other archaeological and paleoenvironmental sites in eastern Africa and thus contribute to a supra-regional reconstruction of the settlement history and paleoenvironment. In particular, our study contributes to close the chronological gap of human occupation in north-eastern Africa around the times of the LGM.

DATA AVAILABILITY STATEMENT

The datasets analyzed for this study can be found at the CRC 806 Database, https://doi.org/10.5880/SFB806.55.

AUTHOR CONTRIBUTIONS

RV and OB developed the project framework within the CRC 806. RV and TN did archaeological excavation and preliminary stone tool analyze. EH performed sediment sampling in the field, sedimentological and geochemical analyses in the laboratory and developed the age-depth model with RStudio. EH developed the manuscript and figures. All co-authors contributed to, read, and approved the paper.

FUNDING

ACKNOWLEDGMENTS

our colleagues from the radiocarbon AMS lab of the University of Cologne for radiocarbon dating. We thank Marianne Dohms and her colleagues from the Institute of Geography of the RWTH Aachen for their help and instructions for sediment color and XRF measurements. We are very grateful Thomas Albert, Degene Bado, Dejenne Degena, Mesfin Gete, Solomon Gitaw, Habir Mohammed Kebir, Mareike Röhl, Christian Schepers, Desta Sinajew, Mehdanit Tamerat, Fitsum Tefera, Minassie Tekelemariam and Thorben Thenbruck for their

participation during various field seasons at Sodicho. Finally, we thank the local residents of Mt. Sodicho for their participation and support in field research.

SUPPLEMENTARY MATERIAL

The Supplementary Material for this article can be found online at: https://www.frontiersin.org/articles/10.3389/feart. 2020.611700/full#supplementary-material.

REFERENCES

Arnaud, F., Révillon, S., Debret, M., Revel, M., Chapron, E., Jacob, J., et al. (2012). Lake Bourget regional erosion patterns reconstruction reveals Holocene NW European Alps soil evolution and paleohydrology. *Quat. Sci. Rev.* 51, 81–92. doi:10.1016/j.quascirev.2012.07.025

Barrón, V., and Torrent, J. (1986). Use of the kubelka–munk theory to study the influence of iron oxides on soil colour. *J. Soil Sci.* 37, 499–510. doi:10.1111/j.1365-2389.1986.tb00382.x

Basell, L. S. (2008). Middle Stone Age (MSA) site distributions in eastern Africa and their relationship to Quaternary environmental change, refugia and the evolution of Homo sapiens. *Quat. Sci. Rev.* 27 (27), 2484–2498. doi:10.1016/j.quascirev.2008.09.010

Benito-Calvo, A., De la Torre, I., Mora, R., Tibebu, D., Morán, N., and Martínez-Moreno, J. (2007). Geoarchaeological potential of the western bank of the Bilate River (Ethiopia). Analele Universităţii din Oradea XVIISeria Geographie), 99–104.

Berhanu, B., Melesse, A. M., and Seleshi, Y. (2013). GIS-based hydrological zones and soil geo-database of Ethiopia. *Catena* 104, 21–31. doi:10.1016/j.catena.2012.12.007

Blaauw, M. (2010). Methods and code for 'classical'age-modelling of radiocarbon sequences. *Quat. Geochronol.* 5 (5), 512–518. doi:10.1016/j.quageo.2010.01.002

Blott, S. J., and Pye, K. (2001). GRADISTAT: a grain size distribution and statistics package for the analysis of unconsolidated sediments. *Earth Surface Processes and Landforms.* 26 (11), 1237–1248. doi:10.1002/esp.261

Bon, F., Dessie, A., Bruxelles, L., Daussy, A., Douze, K., Fauvelle-Aymar, F., et al. (2013). Prehistory of the central main Ethiopian rift (Ziway-Shala basin): establishing the late stone age sequence in eastern Africa. *An. Ethiopie.* 28, 405–407. doi:10.3406/ethio.2013.1552

Bonini, M., Corti, G., Innocenti, F., Manetti, P., Mazzarini, F., Abebe, T., et al. (2005). Evolution of the Main Ethiopian Rift in the frame of Afar and Kenya rifts propagation. *Tectonics* 24, 1. doi:10.1029/2004TC001680

Brandt, S. A., Fisher, E. C., Hildebrand, E. A., Vogelsang, R., Ambrose, S. H., Lesur, J., et al. (2012). Early MIS 3 occupation of Mochena Borago rockshelter, southwest Ethiopian highlands: implications for late Pleistocene archaeology, paleoenvironments and modern human dispersals. *Quat. Int.* 274, 38–54. doi:10.1016/j.quaint.2012.03.047

Brandt, S., Hildebrand, E., Vogelsang, R., Wolfhagen, J., and Wang, H. (2017). A new MIS 3 radiocarbon chronology for Mochena Borago Rockshelter, SW Ethiopia: implications for the interpretation of Late Pleistocene chronostratigraphy and human behavior. *J. Archaeol. Sci. Report.* 11, 352–369. doi:10.1016/j.jasrep.2016.09.013

Brown, E. T. (2011). Lake Malawi's response to "megadrought" terminations: sedimentary records of flooding, weathering and erosion. *Palaeogeogr. Palaeoecol.* 303 (1-4), 120–125. doi:10.1016/j.palaeo.2010.01.038

Chernet, T. (2011). Geology and hydrothermal resources in the northern Lake Abaya area (Ethiopia). *J. Afr. Earth Sci.* 61 (2), 129–141. doi:10.1016/j.jafrearsci.2011.05.006, 2011

Corti, G. (2009). Continental rift evolution: from rift initiation to incipient break-up in the Main Ethiopian Rift, East Africa. *Earth Sci. Rev.* 96 (1-2), 1–53. doi:10.1016/j.earscirev.2009.06.005

Corti, G., Sani, F., Philippon, M., Sokoutis, D., Willingshofer, E., and Molin, P. (2013). Quaternary volcano-tectonic activity in the Soddo region, western

margin of the Southern Main Ethiopian Rift. *Tectonics* 32 (4), 861–879. doi:10.1002/tect.20052

De la Torre, I., Benito-Calvo, A., Mora, R., Martínez-Moreno, J., Morán, N., and Tibebu, D. (2007). Stone age occurences in the western bank of the Bilate River (southern Ethiopia) - some preliminary results. *Nyame Akuma.* 67, 14–25.

Eckmeier, E., and Gerlach, R. (2012). Characterization of archaeological soils and sediments using VIS spectroscopy. *eTopoi. J. Ancient Stud.* 3, 285–290. doi:10.1002/gea.1004

Fisher, E. (2010). *Late Pleistocene technological change and hunter-gatherer behavior at moche Borago rockshelter, sodo-wolayta, Ethiopia: flaked stone artifacts from the early OIS 3 (60–43 ka) deposits.* Gainesville, FL: University of Florida.

Foerster, V., Junginger, A., Langkamp, O., Gebru, T., Asrat, A., Umer, M., et al. (2012). Climatic change recorded in the sediments of the Chew Bahir basin, southern Ethiopia, during the last 45,000 years. *Quat. Int.* 274, 25–37. doi:10.1016/j.quaint.2012.06.028

Foerster, V., Vogelsang, R., Junginger, A., Asrat, A., Lamb, H. F., Schaebitz, F., et al. (2015). Environmental change and human occupation of southern Ethiopia and northern Kenya during the last 20,000 years. *Quat. Sci. Rev.* 129, 333–340. doi:10.1016/j.quascirev.2015.10.026

Folk, R. L., and Ward, W. C. (1957). Brazos River bar [Texas]; a study in the significance of grain size parameters. *J. Sedim. Res.* 27 (1), 3–26. doi:10.1306/74d70646-2b21-11d7-8648000102c1865d

Garcin, Y., Melnick, D., Strecker, M. R., Olago, D., and Tiercelin, J.-J. (2012). East African mid-Holocene wet–dry transition recorded in palaeo-shorelines of Lake Turkana, northern Kenya Rift. *Earth Planet. Sci. Lett.* 331-332, 322–334. doi:10.1016/j.epsl.2012.03.016

Goldberg, P., and Bar-Yosef, O. (1998). "In site formation processes in kebara and hayonim caves and their significance in levantine prehistoric caves." in *Neandertals and modern humans in western Asia.* Editors T. Akazawa, K. Aoki, and O. Bar-Yosef (Boston, MA: Springer US), 107–125. doi:10.1007/0-306-47153-1_8

Goldberg, P., Miller, C. E., Schiegl, S., Ligouis, B., Berna, F., Conard, N. J., et al. (2009). Bedding, hearths, and site maintenance in the Middle Stone age of Sibudu cave, KwaZulu-Natal, South Africa. *Archaeol. Anthropo. Sci.* 1, 95–122. doi:10.1007/s12520-009-0008-1

Griffiths, J. (1972). "Ethiopian highlands,"in *World survey of climatology," in climates of Africa.* Editors H. Landsberg and N.L Amsterda (New York, NY: Elsevier), Vol. 10, 369–381.

Gutherz, X., Jallot, L., Lesur, J., Pouzolles, G., and Sordoillet, D. (2002). Annales d'Éthiopie, De Boc-card/Centre Français des Études Éthiopiennes. *Annales d'Ethiopie* 18, 181–190. doi:10.3406/ethio.2002.1019

Hemming, S. R. (2004). Heinrich events: massive late Pleistocene detritus layers of the north atlantic and their global climate imprint. *Rev. Geophys.* 42, RG1005. doi:10.1029/2003RG000128

Hensel, E. A., Bödeker, O., Bubenzer, O., and Vogelsang, R. (2019). Combining geomorphological– hydrological analyses and the location of settlement and raw material sites – a case study on understanding prehistoric human settlement activity in the southwestern Ethiopian Highlands. *E&G Quaternary Sci. J.* 68, 201–213. doi:10.5194/egqsj-68-201-2019

Herrejón Lagunilla, Á., Carrancho, Á., Villalaín, J. J., Mallol, C., and Hernández, C. M. (2019). An experimental approach to the preservation potential of magnetic signatures in anthropogenic fires. *PLoS One.* 14, e0221592. doi:10.1371/journal.pone.0221592

Hildebrand, E. A., and Brandt, S. A. (2010). An archaeological survey of the tropical highlands of Kafa, southwestern Ethiopia. *J. Afr. Archaeol.* 8 (1), 43–63. doi:10.3213/1612-1651-10152

Hildebrand, E. A., Brandt, S. A., Friis, I., and Demissew, S. (2019). "Paleoenvironmental reconstructions for the Horn of Africa: Interdisciplinary perspectives on strategy and significance," in *Trees, grasses and crops. People and plants in sub-saharan Africa and beyond*. Editors B. Eichorn and A. Höhn (Bonn, DE: Verlag Dr. Rudolf Habelt)), 187–210.

Holliday, V. T., and Gartner, W. G. (2007). Methods of soil P analysis in archaeology. *J. Archaeol. Sci.* 34 (2), 301–333. doi:10.1016/j.jas.2006.05.004

Hunt, A. M., and Speakman, R. J. (2015). Portable XRF analysis of archaeological sediments and ceramics. *J. Archaeol. Sci.* 53, 626–638. doi:10.1016/j.jas.2014.11.031

Inglis, R. H., French, C., Farr, L., Hunt, C. O., Jones, S. C., Reynolds, T., et al. (2018). Sediment micromorphology and site formation processes during the middle to later stone ages at the haua fteah cave, cyrenaica, Libya. *Geoarchaeology* 33 (3), 328–348. doi:10.1002/gea.21660

Iuss Working Group Wrb (2014). *World Reference Base for Soil Resources International soil classification system for naming soils and creating legends for soil maps in World soil resources report*. Rome: FAO, 106, 188.

Ivers-Tiffée, E., and von Münch, W. (2007). "Magnetische werkstoffe," in *Werkstoffe der Elektrotechnik*. Editors E. Ivers-Tiffée and W. von Münch (Wiesbaden (DE: B.G. Teubner Verlag) doi:10.1007/978-3-8351-9088-7_6

Junginger, A., and Trauth, M. H. (2013). Hydrological constraints of paleo-Lake Suguta in the Northern Kenya Rift during the African humid period (15–5 ka BP). *Global Planet. Change.* 111, 174–188. doi:10.1016/j.gloplacha.2013.09.005

Kaniewski, D., Marriner, N., Cheddadi, R., Joel, G., and Campo, E. (2018). The 4.2 ka BP event in the Levant. *Clim. Past.* 14, 1529–1542. doi:10.5194/cp-14-1529-2018

Karkanas, P. (2017). "Chemical alteration,," in *Encyclopedia of geoarchaeology. Encyclopedia of earth sciences series*. Editor A. S. Gilbert (Dordrecht, NL: Springer-Verlag) doi:10.1007/978-1-4020-4409-0_126

Kehl, M., Burow, C., Cantalejo, P., Domínguez-Bella, S., Durán, J. J., Henselowsky, F., et al. (2016). Site formation and chronology of the new Paleolithic site Sima de Las Palomas de Teba, southern Spain. *Quat. Res.* 85 (2), 313–331. doi:10.1016/j.yqres.2016.01.007

Kehl, M., Eckmeier, E., Franz, S., Lehmkuhl, F., Soler, J., Soler, N., et al. (2014). Sediment sequence and site formation processes at the Arbreda Cave, NE Iberian Peninsula, and implications on human occupation and climate change during the Last Glacial. *Clim. Past.* 10 (5), 1673–1692 doi:10.5194/cp-10-1673-2014

Khalidi, L., Mologni, C., Ménard, C., Coudert, L., Gabriele, M., Davtian, G., et al. (2020). 9000 years of human lakeside adaptation in the Ethiopian Afar: Fisher-foragers and the first pastoralists in the Lake Abhe basin during the African Humid Period. *Quat. Sci. Rev.* 243, 106459. doi:10.1016/j.quascirev.2020.106459

Klasen, N., Kehl, M., Mikdad, A., Brückner, H., and Weniger, G.-C. (2018). Chronology and formation processes of the Middle to Upper Palaeolithic deposits of Ifri n'Ammar using multi-method luminescence dating and micromorphology. *Quat. Int.* 485, 89–102. doi:10.1016/j.quaint.2017.10.043

Kröpelin, S., Verschuren, D., Lézine, A.-M., Eggermont, H., Cocquyt, C., Francus, P., et al. (2008). Climate-driven ecosystem succession in the Sahara: the past 6000 years. *Science* 320, 765–768. doi:10.1126/science.1154913.5877

Kuehn, D. D., and Dickson, D. B. (1999). Stratigraphy and noncultural site formation at the shurmai rockshelter (GnJm1) in the mukogodo hills of north-Central Kenya. *Geoarchaeology: Int. J.* 14 (1), 63–85. doi:10.1002/(SICI)1520-6548.199901)14:1<63::AID-GEA5>3.0.CO;2-F

Laskar, J., Robutel, P., Joutel, F., Gastineau, M., Correia, A. C. M., and Levrard, B. (2004). A long-term numerical solution for the insolation quantities of the Earth. *A&A* 428 (1), 261–285. doi:10.1051/0004-6361:20041335

Le Borgne, E. (1955). Susceptibilité magnétique anormale du sol superficiel. *Ann. Geophys.* 11, 399–419.

Marean, C. W., Bar-Matthews, M., Fisher, E., Goldberg, P., Herries, A., Karkanas, P., et al. (2010). The stratigraphy of the middle stone age sediments at pinnacle point cave 13B (mossel bay, western cape province, South Africa). *J. Hum. Evol.* 59 (3-4), 234–255. doi:10.1016/j.jhevol.2010.07.007

Mark, B. G., and Osmaton, H. A. (2008). Quaternary glaciation in Africa: key chronologies and climatic implications. *J. Quat. Sci.* 23, 589–608. doi:10.1002/jqs.1222

Mentzer, S. M. (2017). "Rockshelter settings," in *Encyclopedia of geoarchaeology. Encyclopedia of earth sciences series*. Editor A. S. Gilbert (Dordrecht (NL): Springer-Verlag) doi:10.1007/978-1-4020-4409-0_159

Miller, C. E., Goldberg, P., and Berna, F. (2013). Geoarchaeological investigations at diepkloof rock shelter, western Cape, South Africa. *J. Archaeol. Sci.* 40 (9), 3432–3452. doi:10.1016/j.jas.2013.02.014

Nesbitt, H., and Young, G. (1982). Early Proterozoic climates and plate motions inferred from major element chemistry of lutites. *Nature* 299 (5885), 715–717. doi:10.1038/299715a0

Nicholson, S. E. (2018). The ITCZ and the seasonal cycle over equatorial Africa. *Bull. Am. Meteorol. Soc.* 99 (2), 337–348. doi:10.1175/BAMS-D-16-0287.1

Okrusch, M., and Matthes, S. (2010). *Mineralogie*. Berlin, Germany: Springer-Verlag

Ossendorf, G., Groos, A. R., Bromm, T., Tekelemariam, M. G., Glaser, B., Lesur, J., et al. (2019). Middle Stone Age foragers resided in high elevations of the glaciated Bale Mountains, Ethiopia. *Science* 365 (6453), 583–587. doi:10.1126/science.aaw8942

Reimer, P., Austin, W., Bard, E., Bayliss, A., Blackwell, P., Bronk Ramsey, C., et al. (2020). The IntCal20 northern hemisphere radiocarbon age calibration curve (0–55 cal kBP). *Radiocarbon* 62 (4), 725–757. doi:10.1017/RDC.2020.41

Schepers, C., Lesur, J., and Vogelsang, R. (2020). Hunter-gatherers of the high-altitude afromontane forest – the Holocene occupation of Mount dendi, Ethiopia. *Azania* 55 (3), 329–359. doi:10.1080/0067270X.2020.1792709

Segele, Z. T., Lamb, P. J., and Leslie, L. M. (2009). Large-scale atmospheric circulation and global sea surface temperature associations with Horn of Africa June–September rainfall. *Int. J. Climatol.* 29 (8), 1075–1100. doi:10.1002/joc.1751

Stewart, B. A., and Jones, S. C. (2016). "Africa from MIS 6-2: the florescence of modern humans," in *Africa from MIS 6-2: population dynamics and paleoenvironments*. Editors S. C. Jones and B. A. Stewart (Dordrecht: Springer Netherlands), 1–20. doi:10.1007/978-94-017-7520-5_1

Texier, P. J., Porraz, G., Parkington, J., Rigaud, J. P., Poggenpoel, C., Miller, C., et al. (2010). From the Cover: a Howiesons Poort tradition of engraving ostrich eggshell containers dated to 60,000 years ago at Diepkloof Rock Shelter, South Africa. *Proc. Natl. Acad. Sci. USA.* 107, 6180–6185. doi:10.1073/pnas.0913047107

Tierney, J. E., Lewis, S. C., Cook, B. I., LeGrande, A. N., and Schmidt, G. A. (2011). Model, proxy and isotopic perspectives on east african Humid Period. *Earth Planet Sci. Lett.* 307 (1-2), 103–112. doi:10.1016/j.epsl.2011.04.038

Trauth, M. H., Asrat, A., Duesing, W., Foerster, V., Kraemer, K. H., Marwan, N., et al. (2019). Classifying past climate change in the Chew Bahir basin, southern Ethiopia, using recurrence quantification analysis. *Clim. Dynam.* 53 (5-6), 2557–2572. doi:10.1007/s00382-019-04641-3

Tribolo, C., Asrat, A., Bahain, J. J., Chapon, C., Douville, E., Fragnol, C., et al. (2017). Across the gap: geochronological and sedimentological analyses from the Late Pleistocene-Holocene sequence of Goda Buticha, southeastern Ethiopia. *PLos One.* 12 (1), e0169418. doi:10.1371/journal.pone.0169418

Viste, E., and Sorteberg, A. (2013). Moisture transport into the Ethiopian highlands. *Int. J. Climatol.* 33, 249–263. doi:10.1002/joc.3409

Vogelsang, R., and Wendt, K. P. (2018). Reconstructing prehistoric settlement models and land use patterns on Mt. Damota/SW Ethiopia. *Quat. Int.* 485, 140–149. doi:10.1016/j.quaint.2017.06.061

Willmes, C., Becker, D., Brocks, S., Hütt, C., and Bareth, G. (2017). High resolution köppen-geiger classifications of paleoclimate simulations. *Trans. GIS.* 21, 57–73. doi:10.1111/tgis.12187

WoldeGabriel, G., James, L. A., and Robert, C. W. (1990). Geology, geochronology, and rift basin development in the central sector of the Main Ethiopian Rift. *Geol. Soc. Am. Bull.* 102 (4), 439–485. doi:10.1130/0016-7606 (1990)102<0439:GGARBD>2.3.CO;2

WoldeGabriel, G., Walter, R. C., Aronson, J. L., and Hart, W. K. (1992). Geochronology and distribution of silicic volcanic rocks of Plio-Pleistocene age from the central sector of the Main Ethiopian Rift. *Quat. Int.* 13, 69–76. doi:10.1016/1040-6182(92)90011-P

Wright, D. K. (2017). Humans as agent in the termination of the african Humid Period. *Front. Earth Sci.* 5, 4. doi:10.3389/feart.2017.00004

Xiao, J., Zhang, S., Fan, J., Wen, R., Zhai, D., Tian, Z., et al. (2018). The 4.2 ka BP event: multi-proxy records from a closed lake in the northern margin of the East Asian summer monsoon. *Clim. Past.* 14 (10), 1417–1425. doi:10.5194/cp-14-1417-2018